14:05:53 OCA PAD AMENDMENT - PROJECT HEADER INFORMATION 05/25/93

Active

Project #: E-19-632 Cost share #: Rev #: 2
Center # : 10/24-6-R7152-0A0 Center shr #: OCA file #:
Work type : RES
Contract#: FOREIGN AGREEMENT DATED 3/1/91 Mod #: 2 Document : AGR
Prime #: Contract entity: GTRC

Subprojects ? : N CFDA: N/A
Main project #: PE #: N/A

Project unit: CHEM ENGR Unit code: 02.010.114
Project director(s):
ROUSSEAU R W CHEM ENGR (404)894-2867

Sponsor/division names: AJINOMOTO COMPANY INC / KAWASAKI, JAPAN
Sponsor/division codes: 708 / 014

Award period: 910401 to 930731 (performance) 930731 (reports)

Sponsor amount	New this change	Total to date
Contract value	0.00	105,412.00
Funded	0.00	105,412.00
Cost sharing amount		0.00

Does subcontracting plan apply ?: N

Title: CRYSTALLIZATION OF ASPARTAME

PROJECT ADMINISTRATION DATA

OCA contact: E. Faith Gleason 894-4820

Sponsor technical contact

MR. SATOSHI KUMON
(044)244-7184

AJINOMOTO CO., INC.
CENTRAL RESEARCH LABORATORIES
1-1 SUZUKI-CHO, KAWASAKI-KU
KAWASAKI 210
JAPAN

Sponsor issuing office

MR. SATOSHI KUMON
(044)244-7184

AJINOMOTO CO.,INC.
CENTRAL RESERCH LABORATORIES

FAX: 044-244-9942

Security class (U,C,S,TS) : U ONR resident rep. is ACO (Y/N): N
Defense priority rating : N/A N/A supplemental sheet
Equipment title vests with: Sponsor X GIT

Administrative comments -
MODIFICATION NUMBER 2 PROVIDES A NO-COST EXTENSION TO JULY 31, 1993

GEORGIA INSTITUTE OF TECHNOLOGY
OFFICE OF CONTRACT ADMINISTRATION

NOTICE OF PROJECT CLOSEOUT

Closeout Notice Date 03/10/94

Project No. E-19-632_____ Center No. 10/24-6-R7152-0A0_

Project Director ROUSSEAU R W_____ School/Lab CHEM ENGR_____

Sponsor AJINOMOTO COMPANY INC/KAWASAKI, JAPAN_____

Contract/Grant No. FOREIGN AGREEMENT DATED 3/1/91 Contract Entity GTRC

Prime Contract No. _____

Title CRYSTALLIZATION OF ASPARTAME_____

Effective Completion Date 930731 (Performance) 930731 (Reports)

Closeout Actions Required:	Y/N	Date Submitted
Final Invoice or Copy of Final Invoice	Y	_____
Final Report of Inventions and/or Subcontracts	Y	_____
Government Property Inventory & Related Certificate	Y	_____
Classified Material Certificate	N	_____
Release and Assignment	N	_____
Other _____	N	_____

Comments_____

_____

Subproject Under Main Project No. _____

Continues Project No. _____

Distribution Required:

Project Director	Y
Administrative Network Representative	Y
GTRI Accounting/Grants and Contracts	Y
Procurement/Supply Services	Y
Research Property Managment	Y
Research Security Services	N
Reports Coordinator (OCA)	Y
GTRC	Y
Project File	Y
Other _____	N
_____	N

NOTE: Final Patent Questionnaire sent to PDPI.

CRYSTALLIZATION OF ASPARTAME

Final Report
(Research Period April 1, 1991 – July 31, 1993)

to

Mr. Satoshi Kumon
Section Manager
Central Research Laboratories
Ajinomoto Company, Inc.
1-1, Suzuki-cho, Kawasaki-ku
Kawasaki, 210 JAPAN

by

Ronald W. Rousseau
School of Chemical Engineering
Georgia Institute of Technology
Atlanta, Georgia 30332-0100 USA

and

Kimiyasu Sakamoto
Central Research Laboratories
Ajinomoto Company, Inc.
1-1, Suzuki-cho, Kawasaki-ku

Table of Contents

Table of Contents
(Continued)

1 Introduction

Crystallization of aspartame (L-α-aspartyl-L-phenylalanine methyl ester) is an important step in the recovery and purification of this material. The rate at which mother liquor is separated from the aspartame crystals determines the capacity of a given plant or, alternatively, the size of a new facility. In other words, if the flow of mother liquor through a filter cake is slow, the capacity of an existing crystallizer/solids-liquid separator system is reduced.

Observations (European Patent Application 0091787, 1985) related to the crystallization of aspartame have shown that in conventional systems (those that are well mixed) the crystal habit is of needle-like character and the resulting crystal-liquor separation is difficult. On the other hand, if the cooling aspartame solution is allowed to remain unmixed (static) the resulting slurry consists of "bundles" of aspartame crystals that are more easily separated from the mother liquor. The nature of these bundles has been explored through the use of microscopy (Kishimoto and Naruse, 1987) which showed individual particles to consist of several single crystals neatly stacked on one another. In essence, the crystallization process (that is, allowing the crystallization to occur in a static environment) performs a portion of the solid-liquid separation through the bundling phenomenon.

It is clear that proper and optimal operation of aspartame crystallizers and the advantageous application of static crystallization to other systems requires greater understanding of the factors influencing the phenomenon of bundle formation. Accordingly, the present research program examined the phenomenon from a fundamental perspective. Specifically, the program of study included the following:

1. solubility measurements—Most crystallization phenomena are determined either by the equilibrium properties of solutions of the subject solute or by deviations of a crystallizing system from equilibrium. Accordingly, the solubility of aspartame in aqueous solutions was determined as a function of temperature and other variables.

2. potential differences in crystal forms—The crystals that are produced during static crystallization form bundles with resultant desireable characteristics; needle-like crystals produced in an agitated crystallizer are undesirable. Experiments were performed to obtain these two crystalline species, and the crystals were examined for differences in crystal form.

3. effect of agitation—Agitation of the crystallizer contents during the process of cooling and concomitant crystallization leads to the formation of independent needle-like crystals. Several factors associated with the effect of agitation were examined in a small laboratory crystallizer. Initial guidance in designing the experiments was found in the work of Kishimoto et al. (1989b).

4. the nature of bonding between bundled crystals—The individual crystals comprising the bundles that have been obtained from static crystallization appear to be stable when later agitated in aqueous suspensions and during solid/liquid separation and drying (Kishimoto and Naruse, 1987). The presence of some supersaturation was found by these authors to be necessary for the bundles to be stable. This observation is analogous to findings by Zumstein and Rousseau (1989a) on copper sulfate pentahydrate; they found that crystal agglomeration was enhanced by an increase in supersaturation and magma density (solids fraction in the crystallizing slurry) but decreased by an increase in agitation. We examined the role of these variables in the formation of aspartame bundles.

5. effects of other solutes on crystallization—As an extension of the work on task 4, the nature of the intercrystalline bonds was examined by performing the crystallization in the presence of sodium chloride. Such crystallizations were performed in a dilute solution of electrolyte to shed light on the existence of surface charges on the aspartame crystals. Should electrostatic charges be responsible for the bundling, the effect would be minimized by including an electrolyte in the solution.

   It is suggested that future studies examine the effect of selected surfactants. Zumstein and Rousseau (1989b) found that such agents can influence the habit of amino acid crystals obtained from cooled aqueous solutions and also the character of the slurry of these crystals. For example, addition of a small amount of benzalkonium chloride or didodecyl dimethyl ammonium bromide modified the shape of l-isoleucine crystals obtained by cooling crystallization into a bulkier habit; additionally, the slurry that had been characterized as difficult to handle, because of the formation of crystal agglomerates and the sticking of crystals to crystallizer surfaces, became free flowing with almost no agglomeration. This was thought to be the result of adsorption of tail groups onto hydrophobic crystal faces, leaving the hydrophilic head of the surfactant exposed to the aqueous solution. The surfactants examined must be approved for use in food and/or considered to be useful in explaining observed phenomena.

   Finally, a future study should examine the influence of other species, such as phenyl alanine and other constituents used in the synthesis of aspartame.

2 Solubility of Aspartame

The solubility of APM in water is an important determinant of the yield that can be expected from crystallization. Moreover, as the effect of electrolyte on the formation of bundles is to be examined, experimental determinations of APM solubility in water and aqueous solutions containing 1 wt% NaCl were obtained. The results obtained compared favorably to those of Kishimoto (1989a).

Method

A 100-mL jacketed vessel (d = 40 mm) was used for solubility measurements. Approximately twice the amount of APM required to saturate the solution (as estimated from Kishimoto's empirical equation (1989a)) was added to 80-mL of distilled water. In experiments examining the effect of NaCl on APM solubility, the distilled water was replaced with a 1% NaCl solution. In both cases, the well-mixed slurry was sampled by a syringe, filtered through a 0.45-μm disposable filter disk, and placed into a volumetric flask. A dilution factor was calculated from the weight of filtrate and volume of volumetric flask. The specific gravity of the solution was regarded as 1 g/cm^3.

HPLC conditions used to determine APM concentrations were as follows:

Column:	Whatman Partisphere C18; 12.5 cm; Temp 40°C
Flow rate:	1.5 mL/min
Detector:	Fluorescence (OPA)
Buffer A:	0.05 mol/L phosphate and sodium acetate buffer with 0.5% methanol and 0.5% tetrahydrofuran
Buffer B:	65/35(v/v) methanol/water; gradient of buffer A and B

In order to determine how long systems must be maintained at specified conditions for equilibrium to be achieved, a series of measurements at 40°C were performed at various intervals after mixing APM and solvent. Samples were taken after 5 h, 8 h and 23 h of agitation, and the resulting data showed that equilibrium was reached in about 8 h. That is, after 8 hours there was no change in the concentration of APM in solution regardless of whether the solution was APM in water or APM in an aqueous mixture of 1% NaCl in water. Nevertheless, 24-h period of agitation was used in the solubility experiments.

Results

Solubility data of APM in water and in 1 wt% NaCl solutions are shown in Figure 1 along with data from Kishimoto (1989a). Over the temperature range investigated (20°C to 55°C), measured solubilities in water were 5-10% lower than those of Kishimoto (1989a). One possible cause of these differences is that Kishimoto determined APM concentration by total nitrogen analysis, whereas our measurements were done by HPLC.

The effects of NaCl content on APM solubilities were determined for solutions containing as much as 12 wt% NaCl. The data are shown in Figure 2.

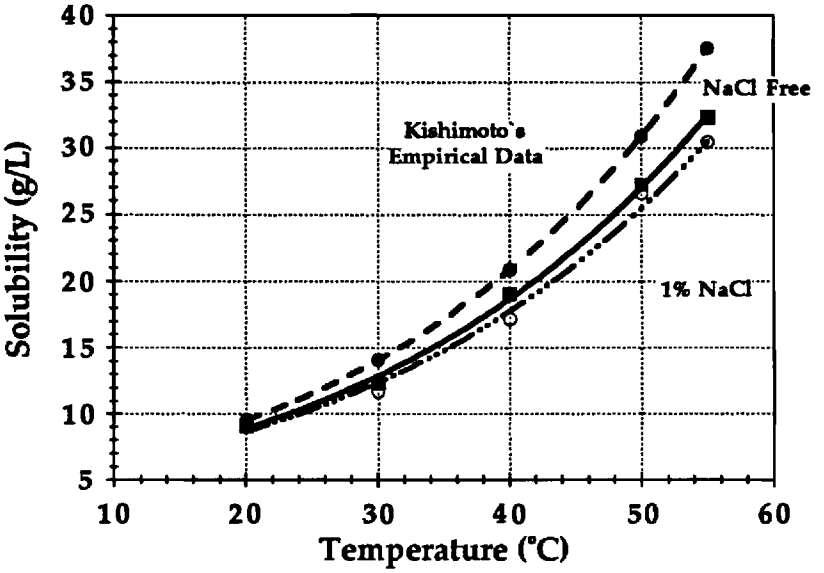

Figure 1: Solubility of APM

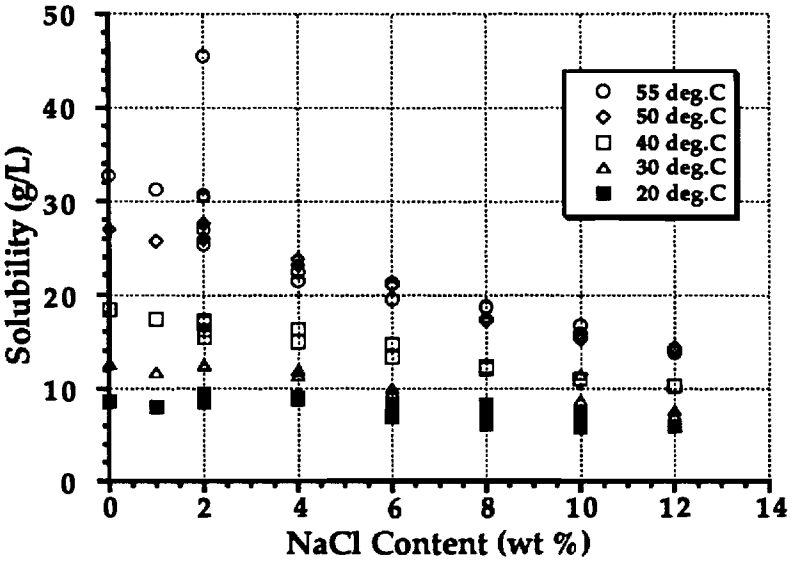

Figure 2: Effect of NaCl on the Solubility of APM

3 Metastable Solubility Limits of APM

When a batch crystallization is performed without the addition of seed crystals, solutions usually exhibit a metastable region reflecting the need for a finite supersaturation in order for nuclei to be formed. In cooling crystallization, the difference between equilibrium temperature and the temperature at which nucleation occurs is referred to as the metastable limit. The work described in this section was performed to determine the metastable limit for APM crystallization under a variety of conditions.

Method

A 500-mL jacketed vessel (d=78 mm) was used as the crystallizer in the present experiments. A particular measured amount of APM powder was dissolved in 500 mL of distilled hot water at 64°C. A magnetic stirrer (1.5 inch in length) was used for agitation. After all of the APM dissolved to give a clear solution, the temperature was maintained for an additional 30 minutes. Then, in order to remove any dust or foreign particulate matter, the solution was passed through a 0.45-μm nylon membrane filter. The filtrate was reheated to 64°C and held at least 30 minutes at this temperature to avoid the risk confounding the experiment with unseen nuclei.

In static crystallization experiments, the magnetic stirrer was removed and the solution was cooled at a predetermined rate. The rate of cooling was controlled by adjusting the temperature of the cooling bath every 2 to 5 minutes by steps of 1°C. For example, in the case of a 12°C/h cooling rate, the temperature of the cooling bath was adjusted by 1°C every 5 minutes; a cooling rate of 60°C/h, was obtained by adjusting the cooling bath temperature by 2°C every 2 minutes.

The key observation in determining the metastable limit is the formation of nuclei, and the temperature at which such nuclei are detected is defined as the metastable limit. By placing a light behind the crystallizer, the Tyndall effect, reflections of light from crystal surfaces in a slurry, was used to enhance the sensitivity in detecting crystals resulting from nucleation.

The system temperature was measured at the bottom corner of the crystallizer by mercury thermometer. This location was chosen because the minimum temperature of the system should be at that corner. (The possibility of temperature distributions in the crystallizer is considered in next section).

Results for Agitated Crystallization

Observations from an experiment in which a solution containing approximately 30 g APM per liter of water was cooled at a rate of 60°C/h are helpful in describing the measurement of metastable limits. The initial solution concentration corresponded to a saturation temperature of approximately 53°C. Although a small number of crystals appeared at about saturation, it was unclear as to whether these were the

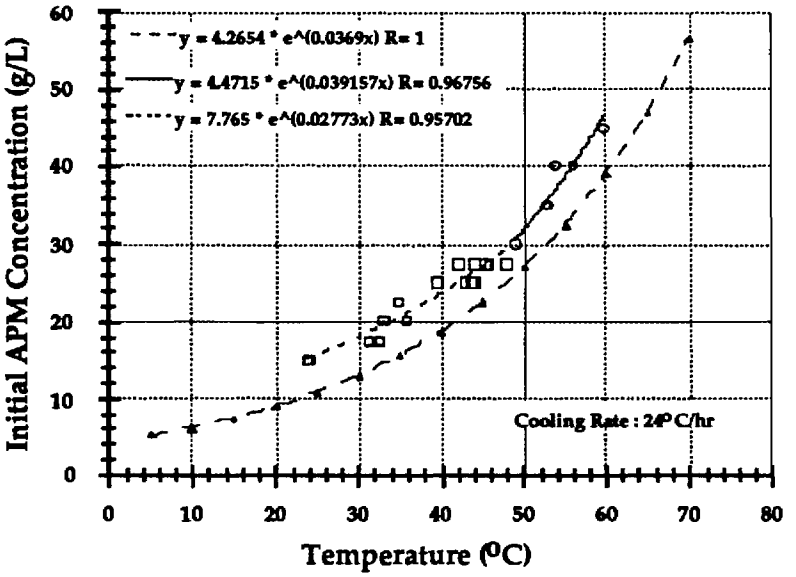

Figure 3: Metastable Limits of APM at a 24°C/h Cooling Rate in an Agitated Crystallizer

result of nucleation or debris remaining in the system. A rapid increase in crystal number occurred at about 48°C, which corresponds to a subcooling of approximately 5°C. The rapid cooling rate used in the experiment made it difficult to determine the precise temperature at which the first crystals were formed. Moreover, even though the solution had been filtered, there still were a few extraneous particles that were observed, even though they had no relation to the experiment. Cooling further to about 44°C, caused the solution to turn cloudy, indicating that there were too many tiny crystals formed to allow light through the slurry. Immediately prior to becoming cloudy, the system clearly showed a significant number of identifiable small crystals. The temperature at which such crystals were observed was defined as the metastable limit for agitated crystallization. This point was difficult to determine, but, fortunately, the temperature difference between the defined metastable limit and the temperature at which the system turned cloudy was at most 0.5°C.

Figure 3 provides results for a series of experiments at varying APM concentrations and in which a cooling rate of 24°C/h was used; otherwise, the experiments were identical to that just described. Shown are the solubility curve for APM and metastable limit determinations for 24 separate experiments. The metastable limit data were fit using a least squares procedure to obtain the correlation shown on the figure.

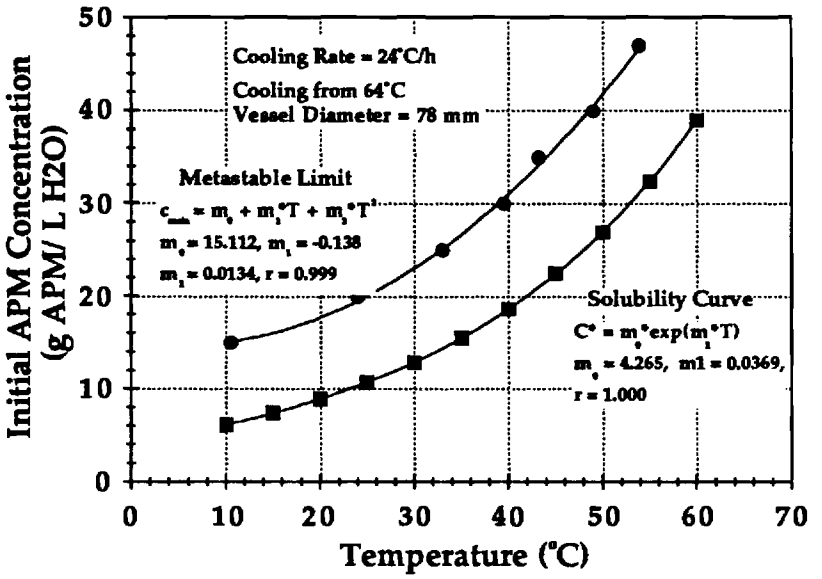

Figure 4: Metastable Limits of APM at a 24°C/h Cooling Rate in a Static Crystallizer

Results for Static Crystallization

Figure 4 shows data obtained in a series of static crystallization experiments in which the cooling rate was 24°C. The solubility of APM is also shown in Figure 4 along with a curve obtained by fitting the metastable limit data using a least squares procedure. It is notable that the metastable limit for static crystallization is significantly wider than that for agitated crystallization. Moreover, the reproducibility of the results from static crystallization appears better than that for agitated crystallization.

The experiments described in the preceding discussion of static crystallization were repeated using cooling rates that varied from 6–60°C. Results obtained are shown in Figure 5. The curves shown for each cooling rate were obtained by fitting a second-order polynomial to the data using a least squares procedure. As shown, increasing the cooling rate increased the width of the metastable region in the low concentration range. At higher concentrations the widths of the metastable regions approach similar values. It is also noteworthy that the metastable limit curve for a 6°C/h cooling rate crosses the metastable limit curves for the other cooling rates. Such behavior is unusual.

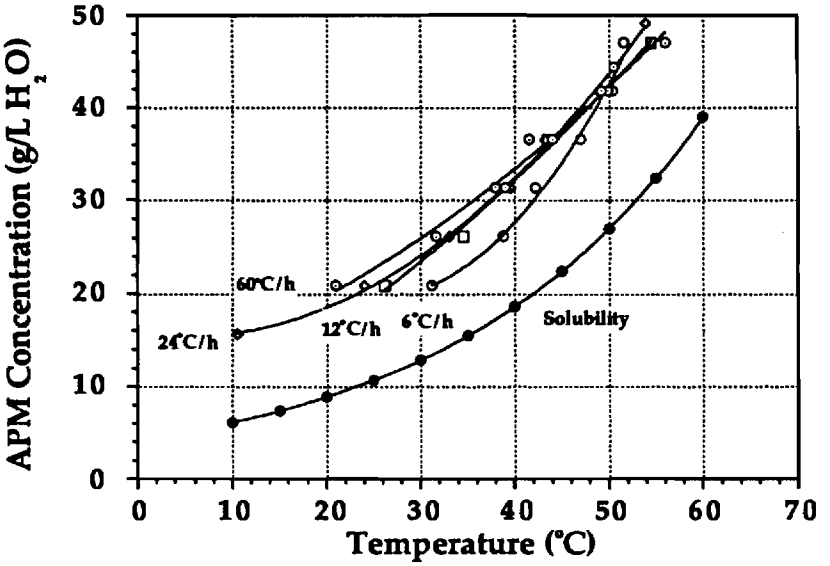

Figure 5: Metastable Limits of APM at Varying Cooling Rates in a Static Crystallizer

Discussion

Several perspectives were taken to assist with interpreting the data taken from both agitated and static crystallization experiments. Clearly, the supersaturation prevailing at the point of nucleation (metastable limit) is an important property of the system. The supersaturation at which the metastable limit was reached was calculated for each experiment reported in Figures 3 and 4 and the results are plotted as a function of saturation temperature in Figure 6.

Using saturation temperature as a dependent variable, as is done in Figure 6, is analogous to using solution concentration. Supersaturation was calculated from $\sigma = (c - c^*)/c^*$, where c is solution concentration c^* is the concentration of APM in a saturated solution at the temperature where nuclei were formed (the metastable limit).

The calculations just described were performed on the data obtained at various cooling rates. The results, which are plotted in Figure 7, show that at low saturation temperatures (low APM concentrations), there is great variation with cooling rate in the metastable supersaturation limit. However, above saturation temperatures of 50°C, the supersaturation at nucleation is relatively independent of cooling rate.

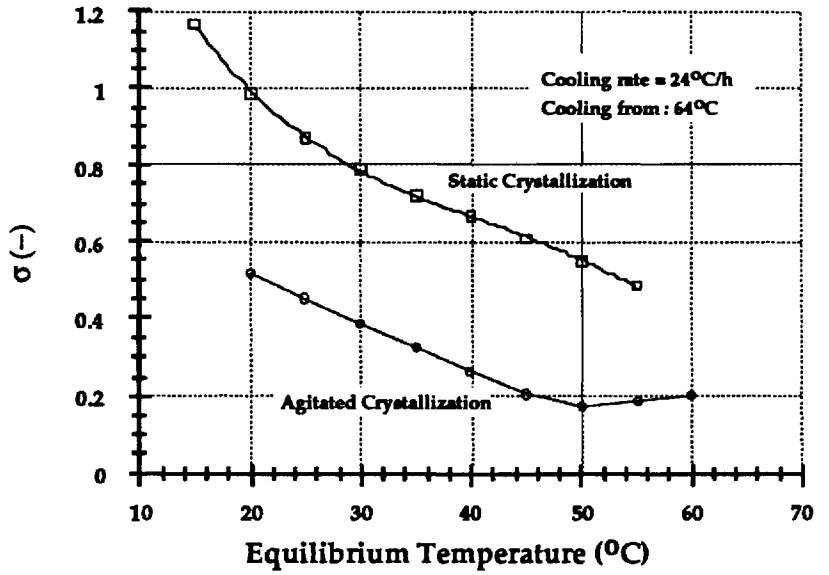

Figure 6: Metastable Supersaturation Limits in Agitated and Static Crystallizations

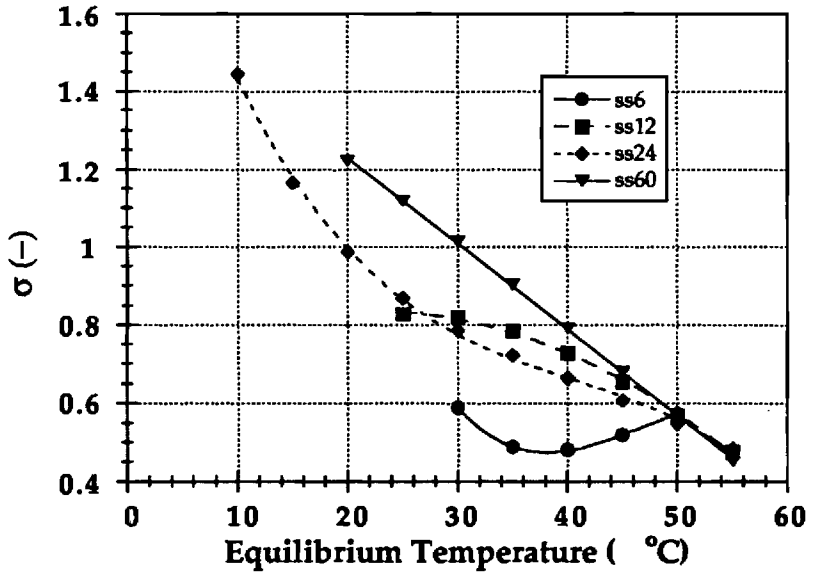

Figure 7: Metastable Supersaturation Limits in Static Crystallizations with Different Cooling Rates

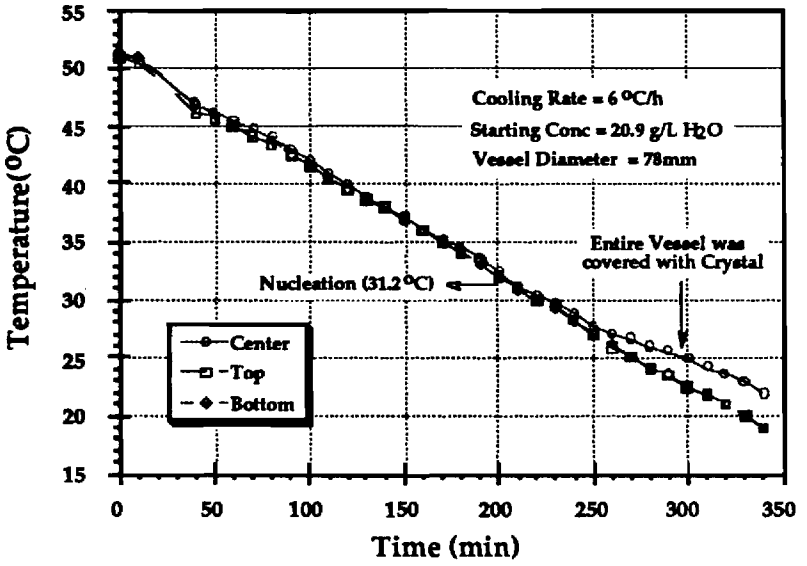

Figure 8: Temperature Distribution in Static Crystallization with an Initial APM Concentration of 20.9 g/L and a Cooling Rate of 6°C/h

4 Thermal Distribution in Static Crystallizer

As mentioned earlier, there was concern about temperature variations within the batch crystallizer used in these and subsequent experiments. Heat is removed from the crystallizer walls and the temperature close to these surfaces may be lower than that in the bulk of the solution. Such variations could influence the phenomena being observed during a given experiment. It was important then that such variation be examined and quantified.

Method

The apparatus used in these experiments was identical to that used in the solubility measurements described earlier. Mercury thermometers were positioned as follows: near the solution surface and adjacent to the crystallizer wall, in the center of the crystallizer wall, and at the bottom corner of the crystallizer. The system was cooled at varying rates as was described earlier.

Results

Figures 8 through 11 show the temperature distributions in the static crystallizer at varying conditions.

In every case shown in these figures, there were insignificant variations of temperature with position in the crystallizer prior to the onset of nucleation. Even

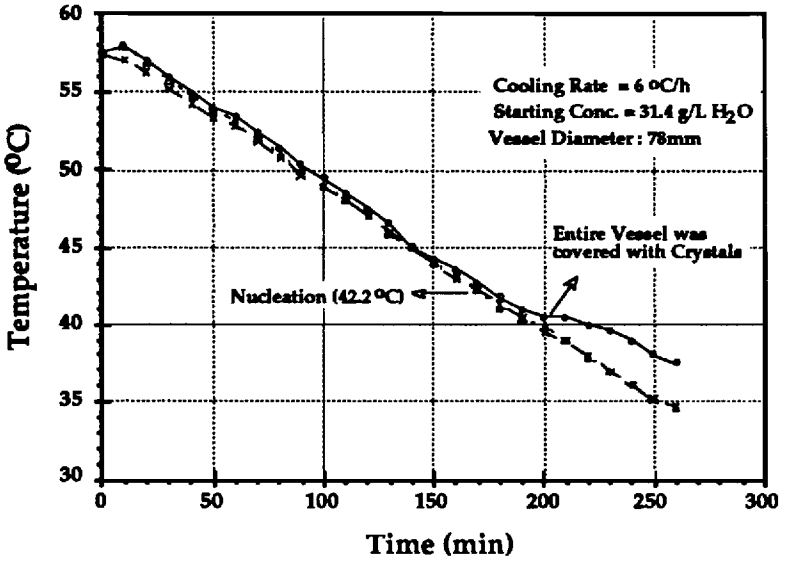

Figure 9: Temperature Distribution in Static Crystallization with an Initial APM Concentration of 31.4 g/L and a Cooling Rate of 6°C/h

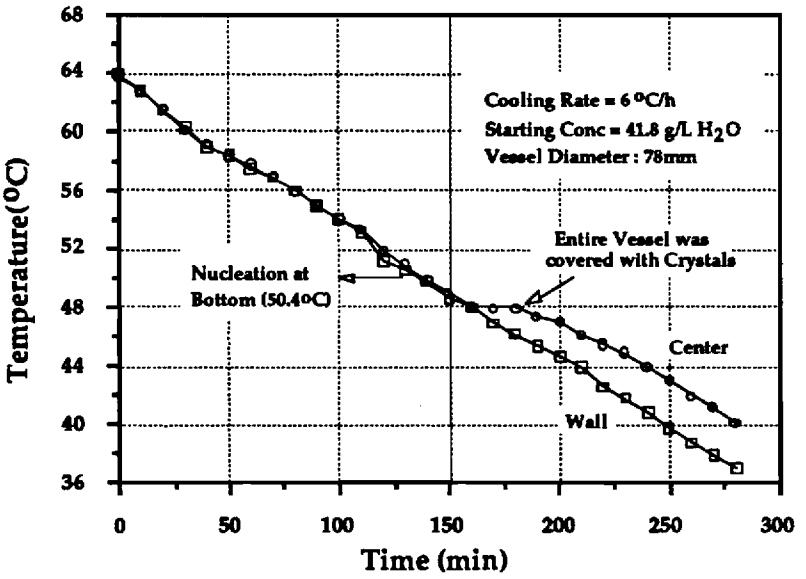

Figure 10: Temperature Distribution in Static Crystallization with an Initial APM Concentration of 41.8 g/L and a Cooling Rate of 6°C/h

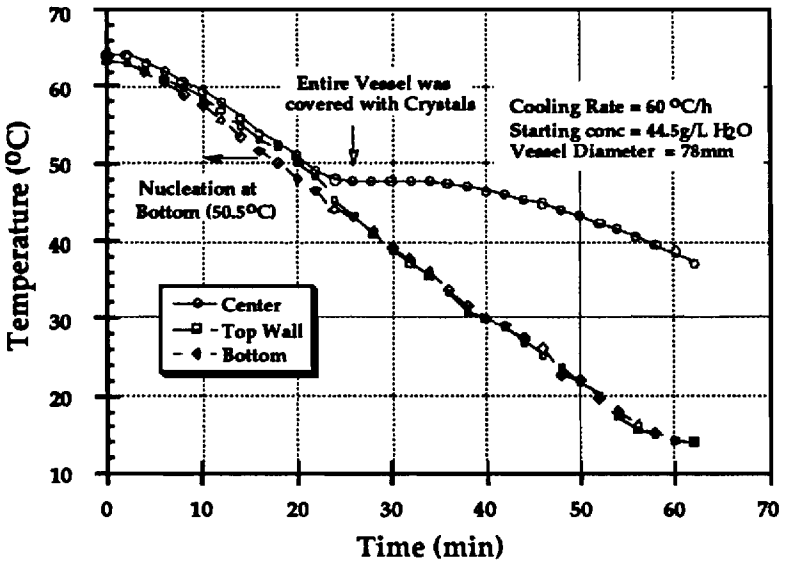

Figure 11: Temperature Distribution in Static Crystallization with Initial APM Concentration of 44.5 g/L and a Cooling Rate of 60°C/h

with the high cooling rate of 60°C (Figure 12), there seems to have been heat transfer, either by conduction or natural convection, to maintain a uniform temperature throughout the system prior to nucleation. Note, however, that after nucleation the difference in temperature between the wall (top and bottom) and the center of the crystallizer increased with increased APM concentration. This is to be expected; the integral heat of solution increases with concentration and there is a larger amount of heat to be removed on crystallization.

5 Supersaturation Release Rate in Agitated Crystallization

In addition to the temperature at which nucleation occurs, the rate at which supersaturation is released through crystal growth is also important. In this section, experiments in which we measured the rate at which APM came out of solution.

Method

The crystallizer used in these experiments was identical to that described earlier. A fixed amount of APM, 15.1 g, was dissolved into 500 mL of distilled water at 60°C. A magnetic stirrer having a length of 1.5 in. was used to agitate the system. The system temperature was maintained at 60°C for at least 30 minutes, and then the solution was passed through a 0.45-μm filter. The filtered solution then was heated again to

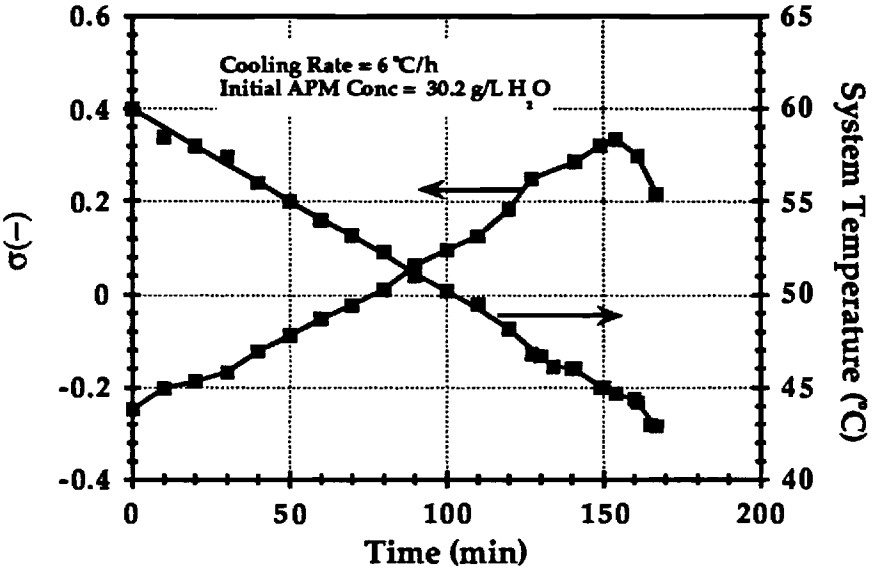

Figure 12: Temperature and Supersaturation Profiles in Agitated Crystallization at a Cooling Rate of 6°C/h

60°C and held at this temperature for 1 hour. It was then cooled at a rate of 6°C/h. After the onset of nucleation, which was determined as described in the section on metastable limits, samples of the solution were withdrawn from the system through a disposable filter. Sampling was continued until the high concentration of crystals in the system caused agitation to cease. The concentration of APM in the samples was determined using the HPLC analytical method which was described earlier.

Results

Figure 12 shows the system temperature and supersaturation (σ) profiles during an experiment involving agitated crystallization in which the cooling rate was 6°C/h. The data show that the cooling rate was linear, as planned, and that the increase in supersaturation is also nearly linear. As expected, a rapid decrease in supersaturation was observed after nucleation of APM, even though the system temperature continued to decrease.

The data from Figure 12 are replotted in Figure 13, which shows measured supersaturation against system temperature; observations of APM crystal formation are noted on the graph. Note that even after nuclei were initially observed and the system had turned cloudy, the supersaturation continued to increase for some period of time.

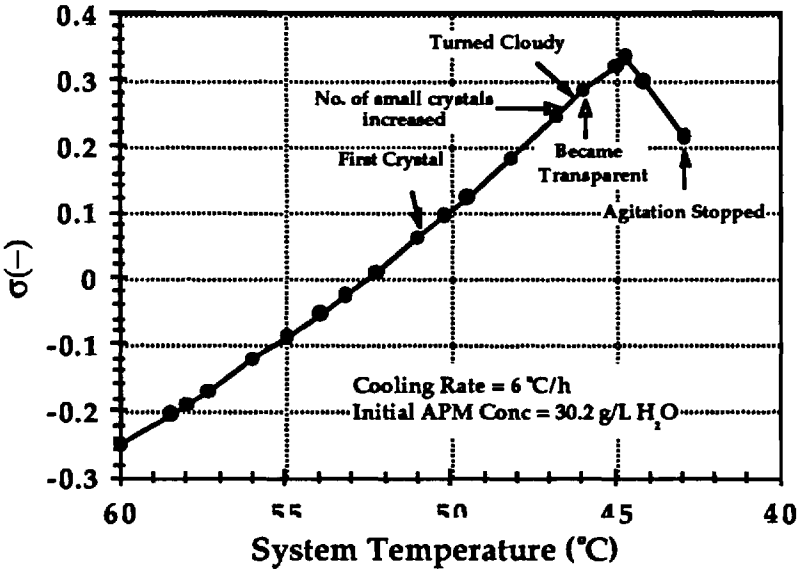

Figure 13: Observations in Agitated APM Crystallization with a Cooling Rate of 6°C/h

Discussion

The supersaturation profile shown in Figure 13 and the associated observation of the onset of nucleation indicate that supersaturation continued to increase, even after nucleation. If sufficient surface area were generated at the initial point of nucleation, the maximum in σ would occur at the nucleation point. However, recognize that primary nucleation rate is a high-order function of supersaturation. This means that as supersaturation increases in the experiment of Figure 13, the nucleation rate increases more rapidly than growth rate, and there is a concomitant increase in surface area available for growth. At the maximum in supersaturation, sufficient surface area has been generated to begin reducing the supersaturation in the system even though the temperature continues to be reduced at the specified rate.

The data from this section suggest the following hypothesis: Once APM crystals have been nucleated in an agitated system, they will never exhibit the bundle-like morphology found to result from the static system. None of the results from subsequent experiments violated this hypothesis. The rapid rate at which supersaturation is released in agitated systems and the large difference between metastable limits in agitated and static systems are thought to be the key phenomenological factors causing the validity of the hypothesis. Put simply, the formation of APM bundles requires a higher supersaturation than that which can be achieved in agitated crystallization.

It is also important to note the differences in nucleation mechanisms in the two type of crystallizations. In static crystallization, only primary nucleation is involved in the formation of APM crystals, but in agitated crystallization, secondary nucleation and even attrition play a significant role. Secondary nucleation by crystal collisions would occur at low supersaturations which would eliminate the possibility of such nuclei forming crystal bundles.

6 APM CRYSTAL SIZE MEASUREMENT

Aspartame (APM) crystals have two kinds of forms which can be formed under different crystallization conditions. These are bundle and needle forms. The bundle form is produced when the crystallization is carried out under static conditions; that is, without mixing. The bundle form tends to grow in only one direction, producing a very long crystal (up to about 60 mm in a vessel having a diameter ϕ of 80 mm) with a narrow width. Because of its shape, this long bundle crystal is easy to break in the length direction, making it difficult to evaluate the crystal size in terms of length. Fortunately, the width of these crystals is a stable dimension, even when the product magma is subjected to as much as 15 minutes of vigorous agitation after crystallization has been completed. This dimension was chosen to characterize crystal size.

No methods for characterizing crystals according to their width have been reported in the literature, although, in principle, this should be relatively straight forward. A set of experiments and method of characterization was developed for this purpose.

Crystallization Procedure

The crystallizer used to perform the necessary experiments was a 600-mL jacketed vessel that was constructed entirely of glass. The temperature of the crystallizer was controlled by water flowing through the jacket and a constant-temperature bath.

The charge to a batch crystallization was prepared by dissolving 23.0 g of APM into 500-ml of water. (Tap water was used in all experiments associated with this part of the program.) The crystallizer and its contents were heated to 72°C, which is about 12°C higher than required to dissolve all of the APM. The solution was held at this temperature for at least 30 minutes after the solution became clear, which was taken to indicate complete dissolution. The magnetic stirrer bar was turned off and removed from the system, and the vessel contents were allowed to begin cooling without any agitation. The cooling rate was set at 60°C/h by changing the temperature set point of circulation bath every 2 minutes by 2°C. After the vessel contents reached 10°C, they were held for an additional 15 hours. The pseudo-solid, sherbert-like slurry then was collapsed and agitated for 15 minutes in order to produce the desired crystal size distribution inside of the crystallizer.

Microscopic Determination of Crystal Dimensions

A randomly selected drop of the mixed slurry was placed on microscope slide, covered by a cover glass, and observed under an optical microscope at a magnification of 40x. Pictures of the crystal picture were taken and enlarged by an instant slide printer (Vivitar, Instant Slide Printer) on Polaroid Type 669 film with the magnification of 3.494x.

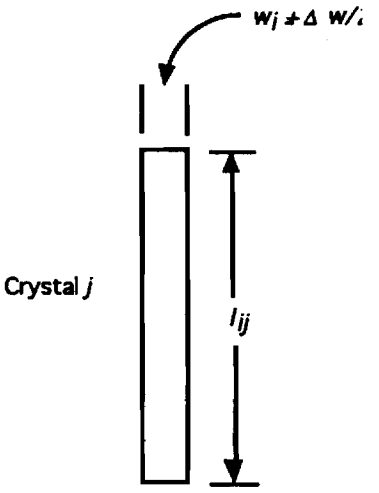

Figure 14: Measurement of Crystal Width

The width and length of all crystals on the photograph was determined using a 6-inch dial caliper (SPI, Manostat) was used for measurement of crystal width and length. All crystals were assumed to be rectangular in shape. A set of results from one crystallization are presented for illustrative purposes in Table 1. These data show the micrometer reading in the first column, crystal width in the second column in mm, the length of crystals having the width given in column two, and the cumulative crystal length.

Mathematical Treatment

Crystals were sized according their width and length. Measurements and the associated nomenclature are illustrated in Figure 1. If the jth crystal has a width between $w_i - \Delta w/2$ and $w_i + \Delta w/2$ and length l_{ij}, then the total length of all crystals having width in the given range is

$$L_i = \sum_{j=1}^{m} l_{ij} \tag{1}$$

where m is the number of crystals having width w_i. The total length of all crystals is

$$L_{total} = \sum L_i \tag{2}$$

Assume that L, the cumulative length function of w, crystal width, is continuous. Then the fraction of the length of crystals in the width size range between w and $w + dw$ is

$$\frac{dL}{L_{total}} = f(w)dw \tag{3}$$

where $f(w)$ is a width density function. The measurements made in the experimental portion of the work were over discrete increments of crystal length and width.

Sample name	920918 (Vessel 1)		
Conditions	Init. APM Conc. : 46.0 g/L H2O		
	Cooling rate : 60 deg.C/hr		
	Nucleation Temp : 49.7 deg.C		
	after 27 minutes, whole system into whi		
	Water source : City Water		
Magnification	**x 40 on slide**		
Sampling method : 15 minutes mixing			
	Sherbet Tower was obserbed		
Observation	*Crystal length : Very long*		
	Number of branching : Very Low		
	Width (mm)	Length Having Given Width	Cumulative Length
4	2.8619E-03	460.111	460.111
5	3.5774E-03	661.355	1121.466
6	4.2928E-03	593.548	1715.014
7	5.0083E-03	810.493	2525.507
8	5.7238E-03	735.553	3261.06
9	6.4392E-03	702.323	3963.383
10	7.1547E-03	484.885	4448.268
11	7.8702E-03	646.739	5095.007
12	8.5857E-03	767.471	5862.478
13	9.3011E-03	783.497	6645.975
14	1.0017E-02	572.12	7218.095
15	1.0732E-02	564.244	7782.339
16	1.1448E-02	502.896	8285.235
17	1.2163E-02	463.622	8748.857
18	1.2878E-02	252.542	9001.399
19	1.3594E-02	358.016	9359.415
20	1.4309E-02	355.108	9714.523
21	1.5025E-02	302.812	10017.335
22	1.5740E-02	178.141	10195.476
23	1.6456E-02	405.49	10600.966
24	1.7171E-02	215.867	10816.833
25	1.7887E-02	203.75	11020.583
26	1.8602E-02	170.723	11191.306
27	1.9318E-02	254.534	11445.84
28	2.0033E-02	239.568	11685.408
29	2.0749E-02	274.688	11960.096
30	2.1464E-02	74.64	12034.736
31	2.2180E-02	38.998	12073.734
32	2.2895E-02	61.696	12135.43
33	2.3611E-02	120.318	12255.748
34	2.4326E-02	132.198	12387.946
35	2.5041E-02	77.84	12465.786
36	2.5757E-02	86.76	12552.546
41	2.9334E-02	48.79	12601.336
42	3.0050E-02	116.004	12717.34
50	3.5774E-02	39	12756.34
		12756.34	

Table 1: Typical Sizing Data on APM Sample

Accordingly, the expressions should be converted as follows:

$$\frac{\Delta L}{L_{total}} = f(w)\Delta w \tag{4}$$

Or, on rearrangement,

$$f(w) = \frac{\Delta L / L_{total}}{\Delta w} \tag{5}$$

The arithmetic mean width, $\bar{w}$, of the distribution function is defined by the following equation:

$$\bar{w} = \frac{\int_0^\infty w f(w)\, dw}{\int_0^\infty f(w)\, dw} \tag{6}$$

Since $\int_0^\infty f(w)\, dw = 1$,

$$\bar{w} = \int_0^\infty w f(w)\, dw \tag{7}$$

The area-weighted mean is

$$\bar{w}_{area} = \frac{\int_0^\infty w^3 f(w) dw}{\int_0^\infty w^2 f(w) dw} \tag{8}$$

Also, the coefficient of variation about the mean, $c.v.$, is defined as

$$c.v. = \frac{\sigma}{\bar{w}} \tag{9}$$

where the variance is given by

$$\sigma^2 = \int_o^\infty (w - \bar{w})^2 f(w)\, dw \tag{10}$$

Again, recognizing that the data in the present study were obtained in discrete form, the mean and variance could be determined from the expressions

$$\bar{w} = \sum_{w_{min}}^{w_{max}} w f(w) \Delta w \tag{11}$$

which on substitution gives

$$\bar{w} = \sum_{w_{min}}^{w_{max}} w \frac{\Delta L}{L_{total}} \tag{12}$$

where w_{min} and w_{max} are the minimum and maximum widths in the data set. The area-weighted mean is

$$\bar{w}_{area} = \frac{\sum_{w_{min}}^{w_{max}} w^3 \frac{\Delta L}{L_{total}}}{\sum_{w_{min}}^{w_{max}} w^2 \frac{\Delta L}{L_{total}}} \tag{13}$$

The variance is now determined as

$$\sigma^2 = \sum_{w_{min}}^{w_{max}} (w - \bar{w})^2 \frac{\Delta L}{L_{total}} \tag{14}$$

Many density functions of naturally occuring substances are described by a gamma distribution,[1] which is given in general terms by the expression

$$f(w) = \frac{1}{\Gamma(a+1)(b/a)^{a+1}} w^a \exp(-aw/b) \tag{15}$$

where the expression $\Gamma(a+1)$ represents the gamma function which is defines by the equation

$$\Gamma(a+1) = \int_0^\infty x^a e^{-x} dx \tag{16}$$

If a is a positive integer, then

$$\Gamma(a+1) = a! \tag{17}$$

A series of experiments were performed to determine the appropriate form of the density function, $f(w)$. Attention was given to the gamma distribution function as a representation of the length density function for APM crystals produced in the present study. Crystals were sized as described earlier and the resulting data were fit using two methods. In the first, the gamma function was used with the parameter a set to an integer value; on testing the fits obtained, it was determined that the best occurred when $a = 1$. That is,

$$f(w) = \frac{1}{b^2} w \exp(-w/b) \tag{18}$$

Figure 2 shows the calculated density function $f(w)$ and the fit of the reduced gamma distribution (Equation 18) to the data. Note that in this expression, there is only one adjustable parameter and it is determined so as to minimize the sum of the squares of differences between model and measured values.

An alternative approach is to use the form of the gamma distribution function (Equation 15) as a guide and to fit the following equation to the data:

$$f(w) = m1 * w^{m_2} \exp(-m_3 w) \tag{19}$$

where m_1, m_2, and m_3 are adjustable parameters. Figure 3 shows a fit of Equation gammamod to the width data on APM from Table 1. Note that the correlation coefficients, R, in the legends of Figures 2 and 3 show a slightly better fit with Equation 19.

Finally, should a fit of the gamma density function in its precise form be desired, a search can be done to evaluate the values of a and b in Equation 15 that provide the best fit to the data. Such a fit is shown in Figure 4.

Because of the way in which crystal width was measured, it is recognized that sampling errors can contribute to erroneous estimates of the width distribution. Such errors can be minimized by ensuring that a sufficiently large sample of crystals is

[1]Both normal and log normal distribution functions were also used to fit the data, but neither was an improvement over the gamma distribution function

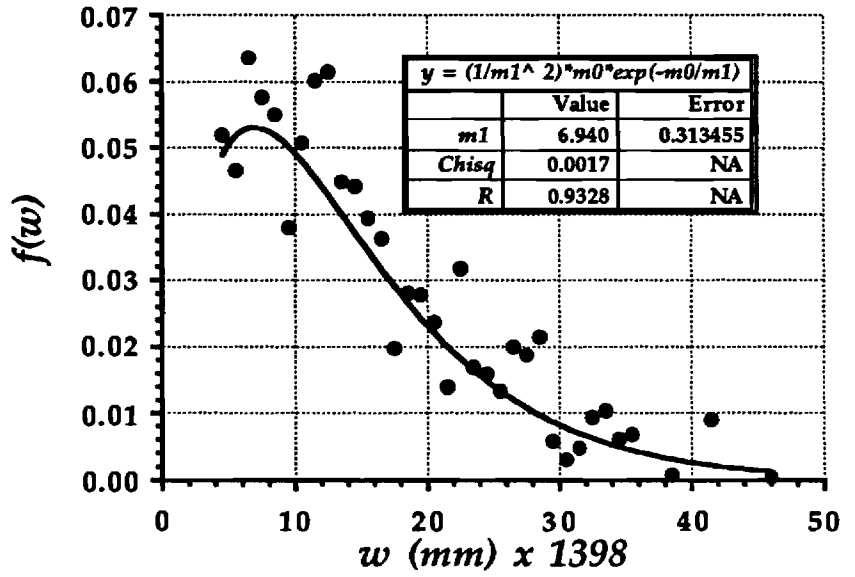

Figure 15: Fit of Reduced Gamma Density Function ($a = 1$) to Measurements

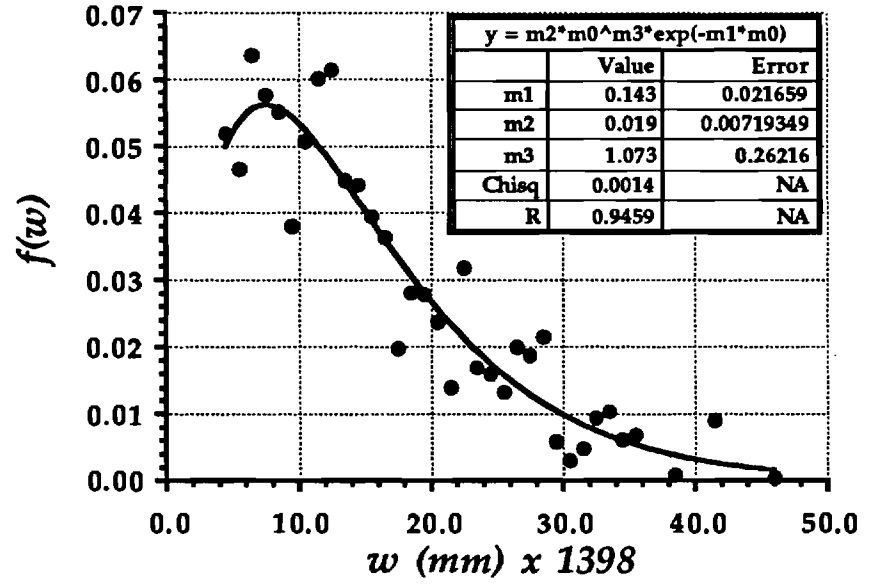

Figure 16: Fit of Empirical Form of Gamma Density Function to Measurements

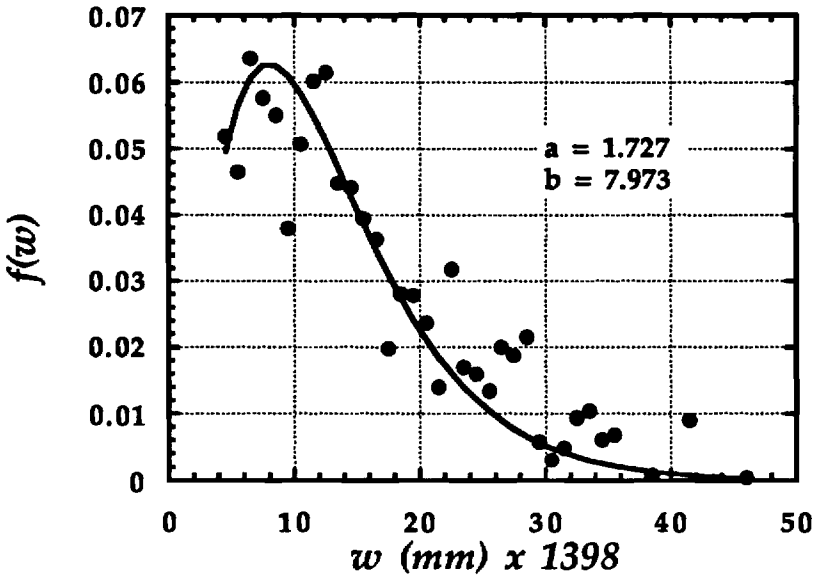

Figure 17: Fit of Complete Gamma Density Function to Measurements

sized. In order to determine the sample size that had to be evaluated to ensure a representative width distribution, a series of measurements were made from random samples taken from an APM static crystallization experiment. The results from each sample were added consecutively to the data fit using Equation 19 and a correlation coefficient was determined for the fit after each sample was added to the data base. Figure 5 shows how the correlation coefficient was poor (significantly less than 1) when the total crystal length measured was low and how it stabilized and gradually approached 1 after the total crystal length exceeded 5,000 mm. This means that to obtain statistically significant information about any batch of crystals, more than 5,000 mm of crystal length must be measured.

A further test of the approach developed here to evaluate the distribution of crystal widths can be obtained by examining the effect of a process variable on a characteristic of the distribution. Figure 6 shows how the arithmetic mean and coefficient of variation of the measured vary with the initial concentration of APM in the solution. The crystals were obtained at a fixed cooling rate of 6°C/h, and the mean width and coefficient of variation were determined from Equations 7 and 9, respectively.

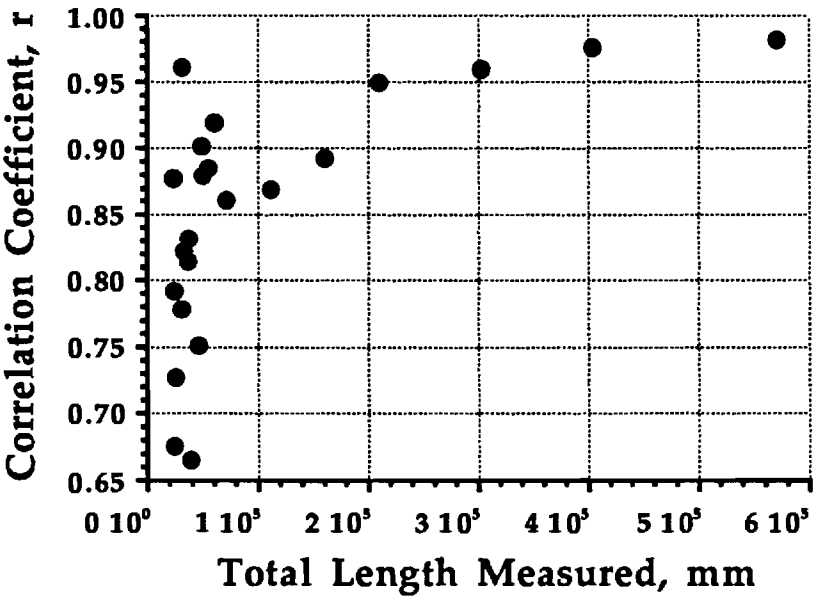

Figure 18: Effect of Total Length Measured on Correlation Coefficient of Fit

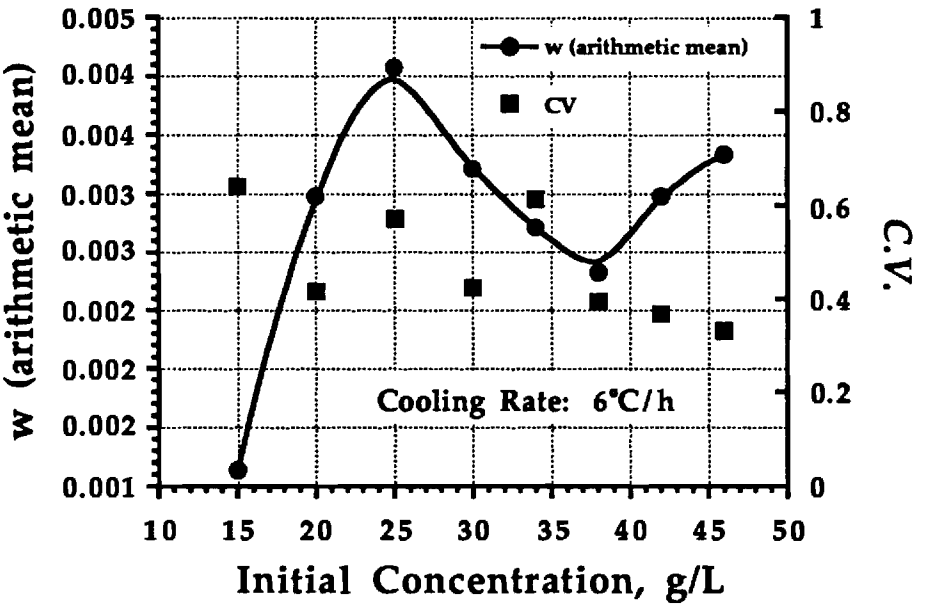

Figure 19: Effect of Initial APM Concenration on $\bar{w}$ and $c.v.$

Conclusions Regarding Crystal Sizing

The analysis of APM crystals from various batch crystallization experiments has been assisted by developing a method of sizing using measured crystal width and length. The crystals themselves have a high length to width aspect ratio when formed, and thus tend to fracture on handling. The method of sizing evaluates the total length of crystals falling in various ranges of widths and results in a width density function that can be used to evaluate key properties of the width distribution, including arithmetic, area-weighted and volume-weighted means, and the coefficient of variation.

The gamma distribution function was chosen to represent the width density function, although it is possible that the width density function could be described by any number of analytical functions. The form of the gamma distribution function was varied so that a reasonable balance between computational simplicity and accuracy was achieved. An empirical modification of the gamma distribution gave a better fit than the reduced gamma distribution and it was easier to evaluate the required parameters than it was for the complete gamma distribution function.

7 Quantification of Mixing Effects on APM Bundle Formation

The need for static conditions to form APM bundles during crystallization had been recognized and was verified by experiments in the current project. A comparison of bundle sizes using the techniques of the previous sections was performed by analyzing data from companion experiments: one in which the agitated crystallization had been used and a second performed using static crystallization. The results are shown in Figure 20. Note that agitation produces a narrow distribution with almost all particles having a width less than 0.001 mm. On the other hand, static crystallization produces a broad distribution with bundles as large as 0.03 mm, more than an order of magnitude larger than those formed in agitated crystallization.

A second set of experiments was performed in which the stirring rate was varied during agitated crystallization. All other conditions remained constant. These results are shown in Figure 21. Clearly, the effect of agitation is profound at all stirrer speeds as there is serious reduction in the mean bundle width at even 10 rpm.

8 Combined Agitation and Static Crystallization

It was not clear whether the requirement of quiescent conditions existed throughout the period of crystallization in order for large bundles to be formed. It was thought that the bundle may be formed at the point of nucleation, and agitation thereafter had no effect on the form of the final product. Alternatively, the bundle might form at a time removed from nucleation so that agitation at nucleation had no effect on bundle formation.

The experiments described here were designed to determine when the future of APM bundles is determined; that is, when the needle-like or bundle character is fixed. In the experiments, the systems were artifically nucleated through the use of one minute of agitation at various supersaturations, all of which exceeded the metastable limit associated with agitated crystallization of APM. It was expected then, that the agitated system would form nuclei at the given conditions. Rather than continuing agitation throughout the experiment, as is the typical case in agitated crystallization, agitation was stopped after a one-minute period. Thereafter, conditions corresponding to static crystallization existed.

Experimental Methods

The crystallizer used in these experiments has been described earlier. The procedure followed was identical to that of static crystallization, except that at selected temperatures that were lower than the equilibrium temperature of 61.98°C, the system was agitated for a period of one minute by turning on the magnetic stirrer with a

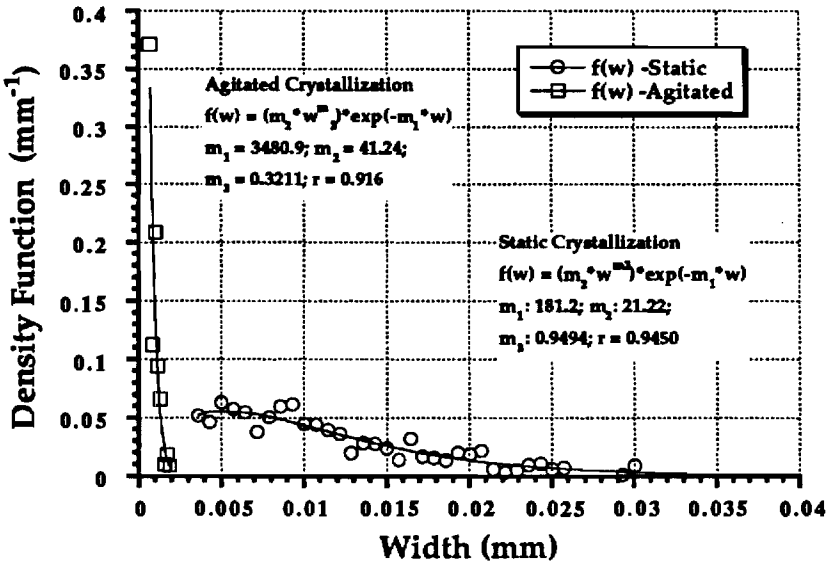

Figure 20: Effect of Mixing on the Distribution of APB Bundle Width

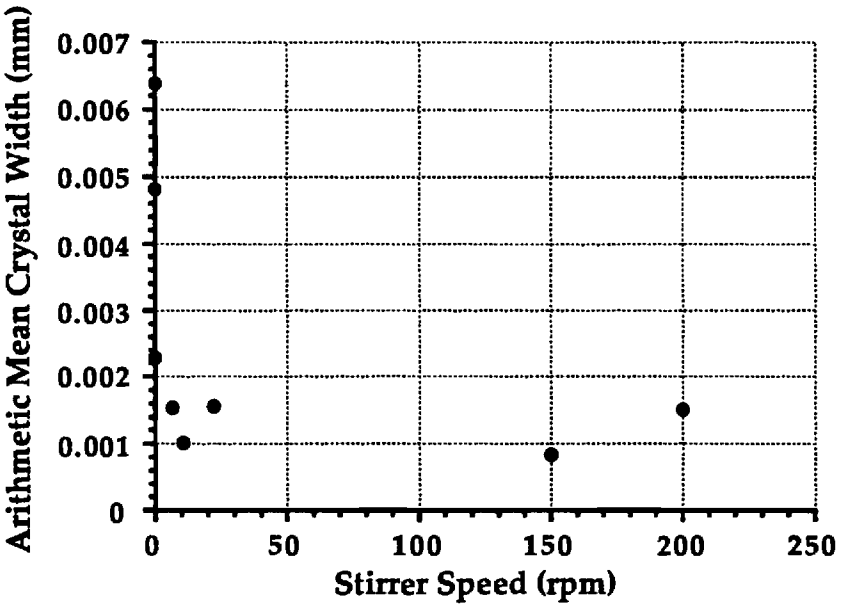

Figure 21: Effect of Stirrer Speed on Arithmetic Mean Bundle Width

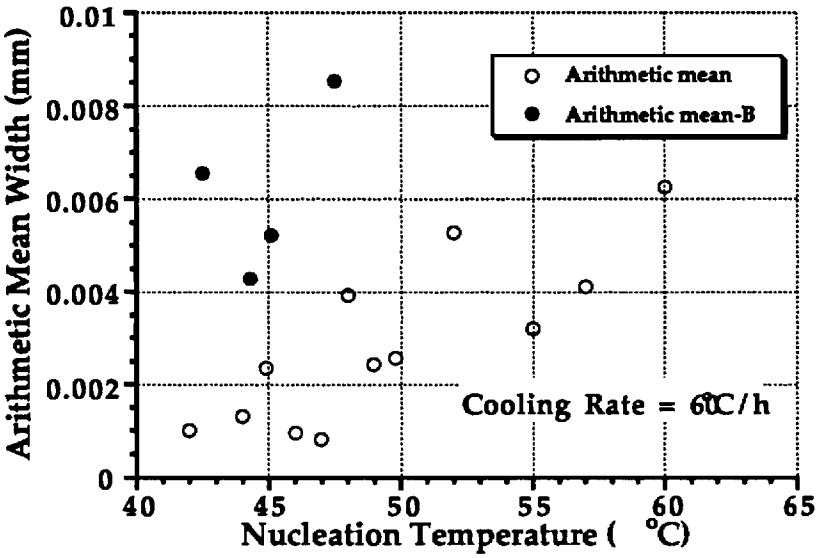

Figure 22: Effect of Temperature at which Nucleation was Initiated by 1 Minute of Agitation or Static (B) Operation

pre-set stirrer speed of 50 rpm. The temperatures at which mixing was started varied from 60°C to 40°C. Nucleation occurred almost immediately with the onset of agitation. When the temperature at which agitation was begun was lower than around 48°C, spontaneous bundle nucleation was observed prior to inititating agitation. All experiments were performed with a cooling rate of 60°C/h.

Results

Table 2 shows all the data obtained in experiments in which there was agitation for a period of one minute after the onset of supersaturation. Figure 22 shows a plot of the width of resulting APM crystals as a function of the temperature at which agitation was initiated. The arithmetic mean was calculated from experimental data using the procedures outlined in Section 6. Included in Figure 22 are data obtained from initiating mixing for one minute at the indicated temperature and those data with darkened circles reflecting true static crystallization. Clearly, initiation of mixing under these conditions reduced the size of the crystal bundle formed.

Although the data are scattered, the increase in crystal width with the temperature at which agitation was begun is thought to be significant; stated in another way, reducing the temperature at which agitation is begun decreases the width of the resulting crystals. Note that since nucleation did not begin until agitation was started,

Table 2: Experimental Results with One Minute of Agitation

T_{agit}	c^*_{agit}	s_{agit}	T_{nuc}	c_{nuc}	s_{nuc}	T_{bundle}	c^*_{bundle}	s_{bundle}	t_{crys}
60.0	39.047	0.076	60.0 (? Needle)	39.047	0.076	47.0	24.168	0.738	19.0
57.0	34.955	0.202	57.0 (? Needle)	34.955	0.202	48.7	25.733	0.632	26.0
55.0	32.468	0.294	55.0 (Needle)	32.468	0.294	49.0	26.019	0.614	12.0
52.0	29.065	0.445	52.0 (? Needle)	29.065	0.445	48.5	25.543	0.644	21.0
49.8	26.799	0.567	49.8 (Needle)	26.799	0.567	47.0	24.168	0.738	14.0
49.0	26.019	0.614	49.0 (Needle)	26.019	0.614	47.1	24.257	0.731	25.0
48.0	25.076	0.675	47.0 (Bundle)	24.168	0.738	47.0	24.168	0.738	19.0
47.0	24.168	0.738	49.0 (Bundle)	26.019	0.614	49.0	26.019	0.614	8.0
46.0	23.292	0.803	47.0 (Bundle)	24.168	0.738	47.0	24.168	0.738	3.0
44.9	22.366	0.878	49.0 (Bundle)	26.019	0.614	49.0	26.019	0.614	2.0
44	21.635	0.941	48.0 (Bundle)	25.076	0.675	48.0	25.076	0.675	2.0
42	20.096	1.090	48.1 (Bundle)	25.169	0.669	48.1	25.169	0.669	0.5
–	–	–	47.5	24.618	0.706	47.5	24.618	0.706	21.0
–	–	–	45.1	22.531	0.864	45.1	22.531	0.864	49.0
–	–	–	42.5	20.470	1.052	42.5	20.470	1.052	47.0
–	–	–	44.3	21.876	0.920	44.3	21.876	0.920	19.0

temperatures (T) in °C; compositions (c) in g/100 mL H_2O; time (t) in minutes

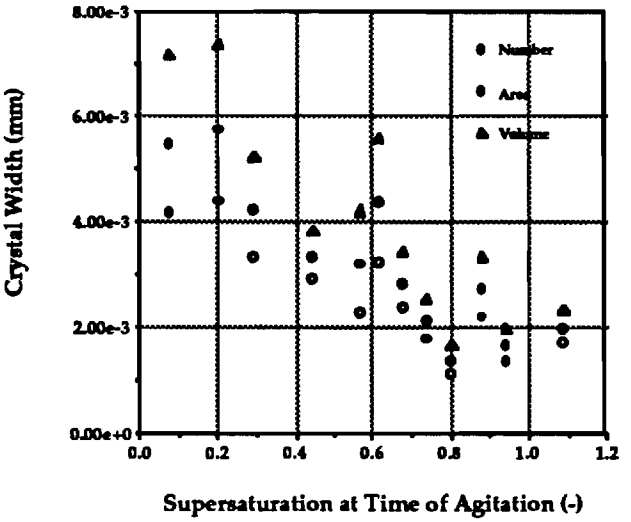

Figure 23: Effect of Supersaturation at Start of 1 Minute of Agitation on APM Bundle Width (Number, Length, Volume Averages)

these results imply that increasing the supersaturation at nucleation decreases crystal width. Figure 23 shows the relationship between the supersaturation at nucleation (the start of agitation) and crystal width. High supersaturation resulted in reduced crystal width, but the data appear to reach a constant value when supersaturation was higher than about 0.8. This corresponds roughly to bundle widths found in true agitated crystallization. On the other hand, nucleation at the same supersaturation (0.8) in true static crystallization produces very large crystals (width $\approx 1.2 \times 10^{-2}$ mm).

Discussion

It is interesting that both needle and bundle crystals were found in the same vessel which had been kept at stationary conditions until the system temperature was lower than 48.0°C. This temperature almost coincides with the nucleation temperature in static crystallization (45.56 ± 1.75°C). Agitation at temperatures greater than 48°C turned the solution into a cloudy suspension, which means there was extensive formation of tiny crystals through secondary nucleation or attrition.

The surface area formed by nucleation with agitation had a profound effect on the time required to produce sufficient crystals to fill the crystallizer. Such filling was reflected by the formation of a crystal mass that had sufficient structure to encompass all of the system and not all observation of any solution within the crystallizer, even when the vessel was tilted. Figure 24 shows a plot of the time to form such a structure as a function of the temperature at which agitation was initiated for a one-minute

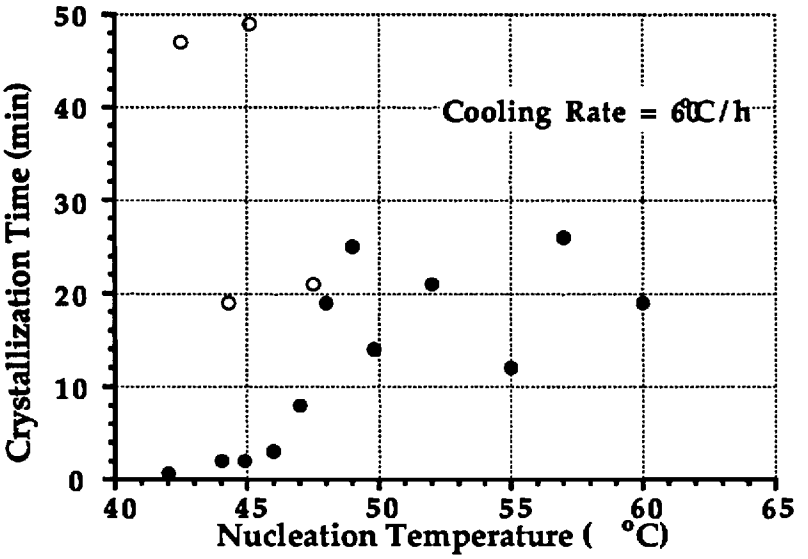

Figure 24: Effect of Temperature at which Nucleation was Initiated by 1 Minute of Agitation or Static (open circles) Operation on the Time to Completely Fill System with Crystals

period.

As shown in Figure 24, the system fills with crystals more than twice as fast when one minute of agitation is initiated at temperatures below 48°C than when such temperature occurs higher temperatures. Nucleation in static crystallization at the given conditions also occurs at about 48°C. The time for the static crystallizer to fill with crystals is much greater than that for agitated crystallization.

The growth of APM crystals is enhanced by the greater surface area presented as a result of secondary nucleation or attrition. Moreover, the greater growth rates encountered in systems that are agitated may prevent an ordering required for bundle formation. Such ordering may occur through a variety of mechanisms, and be disrupted through mixing.

The conclusions that can be drawn from the work described in this section are as follows: (1) APM crystals form in bundles only when crystallization is carried out under completely static conditions at which spontaneous nucleation can occur. (2) Crystals formed under agitated conditions never form bundles.

9 Effects of Initial APM Concentration and Cooling Rate on Crystal Size in Static Crystallization

The concentration of APM in solutions at the time of crystallization may affect the size distribution and form of recovered crystals. In the present section, we describe observations from experiments in which both APM concentration and rate of cooling were varied. The key concern was the mean size of APM crystals, and the APM concentrations investigated ranged from 15 g/L to 54g/L while cooling rates were 6, 24, and 60 °C/h.

Experimental Methods

A 600-mL jacketed vessel with an internal diameter of 80 mm was used as a crystallizer. An appropriate amount of APM was dissolved to provide the desired solution concentration. The solution was agitated by a magnetic stirrer and heated to well above the saturation temperature of the solution. In all cases, concern about the thermal stability of meant that the solution was held at an elevated temperature for only 30 min after complete APM dissolution.

The system was then cooled at a desired rate by manually changing the set point on the circulating bath used to control the crystallizer temperature. A mercury thermometer positioned at the bottom corner of the crystallizer was used to monitor the system termperature. The nucleation temperature, defined as the temperature at which the first APM crystal was observed, was determined. Assistance with this observation was provided by placing a light behind the crystallizer and using the resulting Tyndall effect.

Results

Figure 25 shows the effect of the initial APM concentration on crystal width for the three investigated cooling rates. In every case, a lower initial concentration resulted in smaller crystals, but there were variations with cooling rate in the magnitude of the effect of initial concentration. For example, the initial concentration had a greater impact on crystal width when the cooling rate was 60 °C/h than when either 6 °C/h or 24 °C/h was used. In addition, it appears that the effect of solution concentration on crystal went exhibited a maximum at around 46 g/L when the cooling rate was 60 °C/h.

The coefficient of variation among crystal widths was also determined for the three cooling rates, and the data are shown in Figure 26. In general, the initial concentration had a relatively small influence on coefficient of variation.

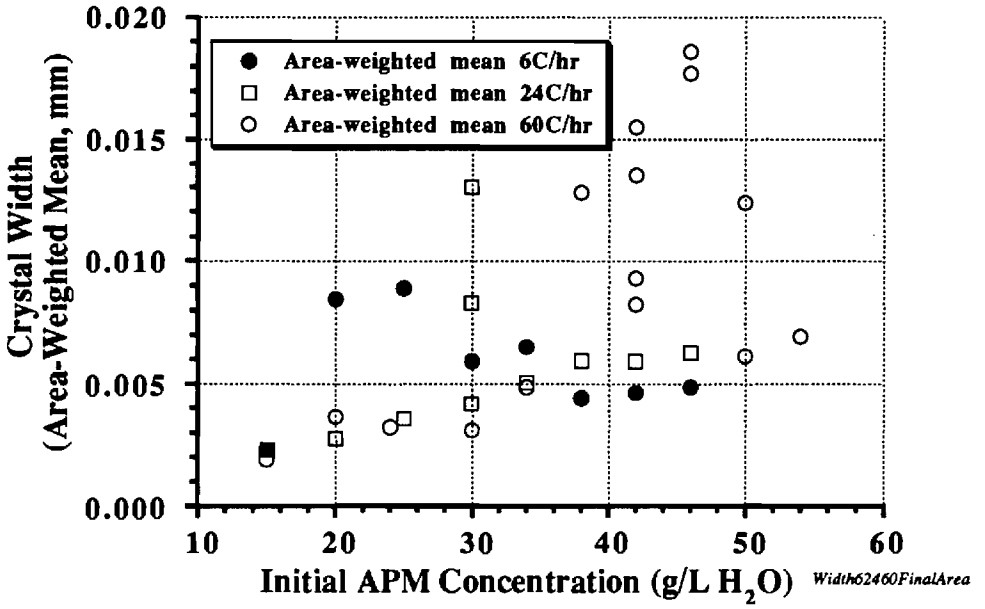

Figure 25: Effect of Initial APM Concentration on Crystal Width

So as to quantify the supersaturation at which nucleation occurred, experiments were performed to determine the metastable limit of APM solutions. The data, along with APM solubility, are shown in Figure 27. It should be recognized that these data are complimentary to those discussed in Section 3, which were obtained under somewhat different conditions.

The data from Figure 27 were used to determine the supersaturation at nucleation for the given experiments. Supersaturation, σ, is defined by

$$\sigma = \frac{c - c*}{c*} \tag{20}$$

where c is the solution concentration at the system conditions and $c*$ is the concentration in a saturated solution at the nucleation temperature. The results are given in Figure 28 which shows the supersaturation at nucleation as a function of the temperature at which nucleation occurred.

The above analysis was used to examine the potential influence of supersaturation and temperature on nucleation and growth kinetics. Recognize that these two phenomena are paramount in determining the size of individual crystals, and information regarding their behavior would lead to a better understanding of APM crystallization.

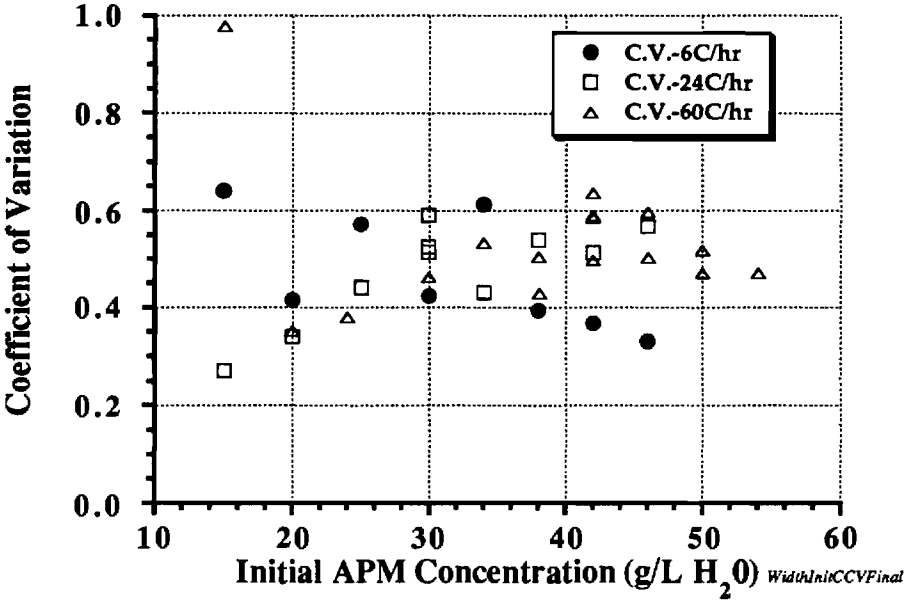

Figure 26: Effect of Initial APM Concentration on Coefficient of Variation

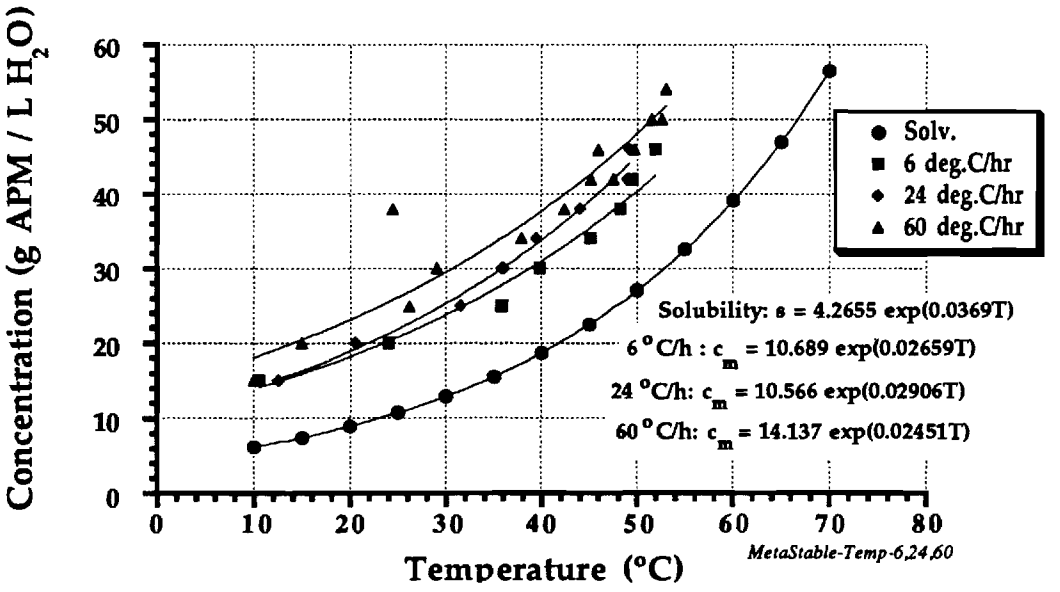

Figure 27: APM solubility and metastable limits

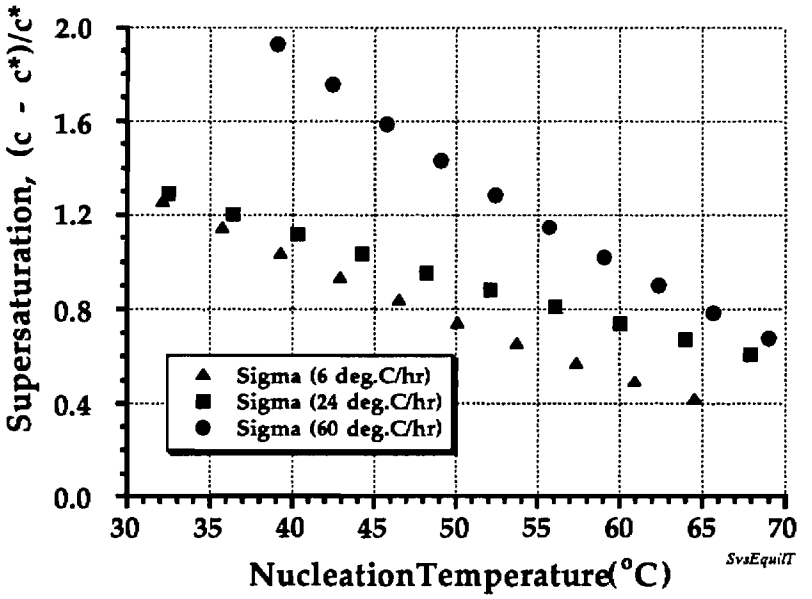

Figure 28: Supersaturation and Temperature of APM Nucleation

The primary nucleation rate B° is given by the theoretically derived expression

$$B^\circ = A \exp\left\{-\frac{16\pi\sigma v}{3k^3T^3[\ln(s+1)]^2}\right\} \tag{21}$$

where A is a constant, σ is interfacial free energy per unit area of the nuclei, v is molar volume, k is the Boltzmann constant, and s is supersaturation.

As only T and s are variables for the experiments performed in the present study, Equation 21 can be rewritten as

$$B^\circ = A' \exp\left\{-\frac{1}{T^3[\ln(s+1)]^2}\right\} \tag{22}$$

If the temperature at nucleation can be used as T in Equation 22, the relationship between T and s for APM can be determined from Figure 4. For example, at the 60°C/h cooling rate, the supersaturation and temperature at nucleation are related by the expression

$$s_{nuc} = 27.68 - 0.145T_{nuc} + 1.919 \times 10^{-4}T_{nuc}^2 \tag{23}$$

where T_{nuc} is in Kelvin. Substituting the relationship from Equation 23 into Equation 22, a normalized nucleation rate can be calculated and used to show the effect

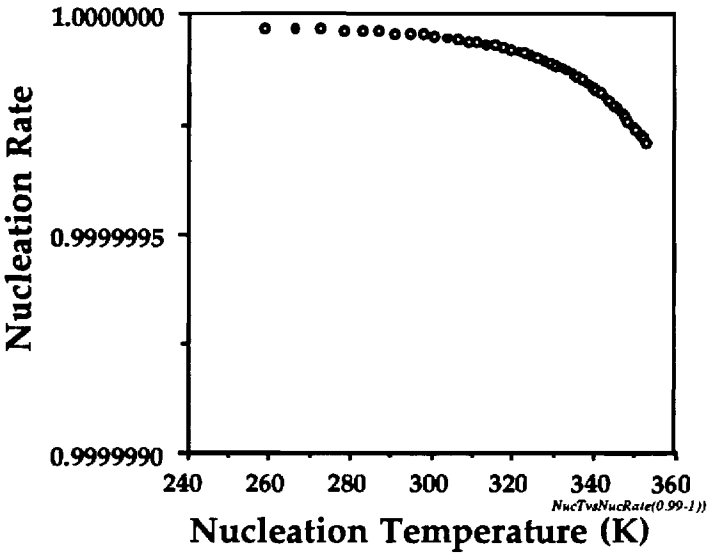

Figure 29: Effect of T on APM Nucleation Rate

of temperature on nucleation rate. The results of such calculations are shown in Figure 29 and demonstrate that the effect of temperature is small.

The dependence of growth kinetics on temperature and supersaturation may be expressed by the empirical relationship

$$G = k_g s^g \tag{24}$$

where k_g is a growth rate constant and $1 < g < 2$. The influence of temperature on the rate constant can be expressed in terms of an Arrhenius relationship:

$$k_g = k_g^\circ \exp\left(-\frac{\Delta E_g}{RT}\right) \tag{25}$$

where k_g° is a temperature-independent growth constant and ΔE_g is the activation energy for crystal growth. Combining these two equations gives

$$G = k_g^\circ \exp\left(-\frac{\Delta E_g}{RT}\right) s^g \tag{26}$$

The activation energy is dependent on both solute and solvent, and it is assumed to be independent of temperature. Unfortunately, there is no way to predict ΔE_g nor are there good experimental values available for the crystallization of APM from aqueous solutions. Accordingly, the influence of temperature on growth rate was determined for several values of activation energy, ranging from 1 to 10 kcal/mol. The results are shown in Figure 30. Note that when ΔE_g is less than 3–5 kcal/mol, the

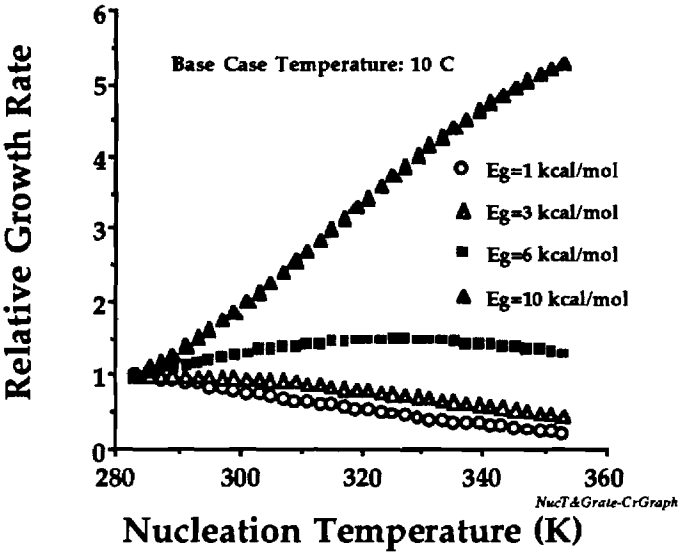

Figure 30: Effect of T on APM Relative Growth Rates

relative growth rate decreases with increasing temperature; one the other hand, at higher values it increases with temperature. These seemingly conflicting predictions are due to the fact that at higher nucleation temperatures the temperatures at which growth is occurring are lower. In other words, increasing temperature increases the rate constant k_g in Equation 24 but it decreases the driving force s.

The results of this analysis explains that the low activation energy for growth of APM crystals leads to an increase in growth rate as the temperature of nucleation goes down. Furthermore, lower initial APM concentrations in solution leads to lower nucleation temperatures and, concomitantly, higher supersaturations at nucleation.

10 Effect of NaCl on APM Crystallization

It had been proposed in the report of September 1992 that the addition of an electrolyte, such as sodium chloride, would test a possible mechanism by which APM bundles are formed in static crystallization. The hypothesis that would be tested suggested that bundle units were attracted to one another by electrostatic charges. The addition of an electrolyte would eliminate the importance of such attractive forces and result in smaller APM particles. In the experiments discussed here, NaCl was the electrolyte chosen for testing, and the effects of NaCl on APM solubility, the metastable limits, and resultant crystal size were examined.

Experimental Methods

A number of 600-mL jacketed vessels, each having a diameter of 80 mm, were used as the crystallizers. Water used to control the temperature of these vessels flowed in series from a cooling bath through the jackets of each vessel. Specific amounts of NaCl were added into 300 mL of tap water, and 12.6 g of APM powder was dissolved into the vessel with agitation by magnetic stirrer. The temperature of this solution was raised to 72°C and held constant for at least 30 minutes after the solution became clear. The vessel were cooled at a rate of 60 °C/h by reducing the set-point temperature of the cooling bath by 2°C every 2 minutes. This cooling rate was so rapid that sometimes cubed ice was necessary to get the desired cooling rate. The temperature of the vessel contents was monitored by mercury thermometer and recorded every 2 minutes. Nucleation temperature and crystallization time, which is defined as the period between nucleation and when the entire system appeared white (no mother liquor was observed when the vessel was tilted), were recorded.

Results

Figure 31 shows that as the concentration of NaCl in the crystallizing solution increased, the width of the resulting APM particles decreased. Even a concentration as low as 0.25 wt% NaCl reduced the particle width. Possible explanations of the observations include the following:

1. Dissolved Na^+ and Cl^- ions disperse the surface static charge on the APM crystal.

   From the correlations of solubility to NaCl concentration at various temperatures, the solubility at a given NaCl concentration and temperature were calculated and used to determine the supersaturation at the point of nucleation for a series of experiments. It was determined in these experiments that the effect of NaCl was to increase the supersaturation at which APM nucleation occurred. The supersaturation at nucleation for an NaCl-free APM system is between 0.6

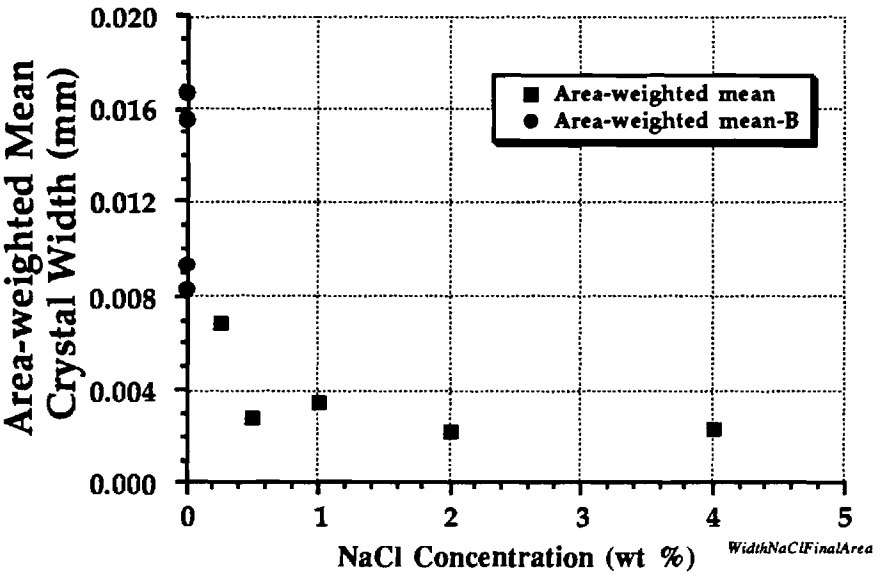

Figure 31: The Effect of NaCl on APM Crystal Width

Table 3: Ratio of NaCl and APM Molecules

NaCl (wt%)	NaCl molecules/APM molecule
0.25	0.598
4.00	9.573

and 1.0. (Recall that supersaturation s is defined as

$$s = \frac{c - c^*}{c^*} \tag{27}$$

However, once NaCl was added to the system at a concentration of 4 wt%, the supersaturation for nucleation increased to around 1.6; that is, it almost doubled. From the point of view of classical nucleation theory, this means that the interfacial energy has been significantly increased with the addition of NaCl.

Table refSaltVsAPM shows the ratio between number of the electrolyte ions and APM molecules. It shows that even the lowest NaCl concentration from the experimental conditions could cancel at least 50% of the charge on an APM molecule. For the 4.0 wt% NaCl system, the static charge should be completely neutralized. Since electrostatic forces are among the strongest and they can

have a long-range effect, canceling the surface change by Na^+ or Cl^- ions might be the main reason of requiring high supersaturation at nucleation.

2. The large size of hydrated Na^+- and Cl^--ion clusters reduces the mobility of APM molecules moving to the growing step on the crystal surface.

   If Na^+ and Cl^- ions do not cancel the surface charge directly, these ions should be extensively hydrated in aqueous solutions. Such hydration will reduce the amount of free water for APM dissolution and also affect mobility of the APM molecule. These two possibilities would have conflicting effects on the nucleation of APM crystals: The former would increase APM concentration, thereby making nucleation easier (the temperature at which nucleation occurs would increase). The latter makes nucleation more difficult since the chances of collision between free molecules and forming nuclei are decreased. The fact that as the NaCl concentration increased, the required supersaturation at nucleation increased supports the theory that Na^+ or Cl^- hydrates have more affect on solute mobility than on solute concentration.

3. There is a change in the hydrophobicity of the surface of APM crystals.

   If the APM crystal surface is considered to be a mosaic of charged hydrophilic and uncharged hydrophobic components, the effect of available counterions on the overall nature of the surface might be quite complex. One possibility could be that every surface charge is canceled by Na^+ or Cl^- ions, and the hydrophobicity of the surface would be increased. Then, if the bundling phenomenon were due to strong hydrophobic interactions between individual crystals, the particle size would increase with the presence of NaCl addition. As this was not the result observed in the experiments, it is possible to reject this mechanism as a factor in bundle formation.

11 The Use of Seed Crystals

The bundling phenomenon that is important in APM crystallization might be observed only if crystals are formed by a primary nucleation mechanism. If that is true, then seeding an APM crystallizer will not produce conditions necessary for the formation of crystal bundles. Such a possibility was examined and is reported in the present section.

In the experiments, crystals of APM obtained from agitated crystallization were added as seed crystals to batch runs. Addition of the seed crystals occurred at various times during the cooing process, ranging from seed introduction at 43°C to 62°C, the latter of which corresponded to saturation temperature.

Experimental Methods

Seed Crystal Preparation

Jacketed, 600-mL vessels having a diameter of 90 mm were used as the crystallizers in the present experiments. The vessel had an anchor, T-shaped paddle agitator (80 mm width by 50 mm length) which was turned by a gear-drive motor. The stirrer speed was 150 rpm. A cooling rate of 24°C/h) was used in the experiments. This vessel was cooled until the contents were at 10°C, and the resulting slurry was held in a refrigerator at 4°C until used to seed the crystallizers.

Seeded Static Crystallization

A specific amount of APM (21.0 g) was dissolved into 500 mL of city water giving an APM concentration of 42.0 g/L H_2O. The system temperature was maintained at at 70°C for at least 30 minutes after all visible crystals disappeared. The vessel was cooled without mixing to 10°C at a rate of 60°C/h. It was necessary to add ice to the cooling unit reservoir to obtain this rate of cooling.

At a specific preselected temperature, 1 mL of APM slurry (obtained from the above-mentioned agitated crystallization) was dropped into the system from a disposable syringe. An attempt was made to spread the seed crystals throughout the entire vessel. Addition of the seed crystals was accomplished over a period of less than 15 seconds.

The onset of nucleation was determined at the given conditions and the temperature at which crystals were first observed by the naked eye was referred to as the nucleation temperature, T_{nuc}. After 16 hours of continuous cooling, the APM crystal magma was recovered by turning the vessel over and allowing it to flow onto a platter. Some of the crystals were in a sherbet tower and the others were in a collapsed slurry. When a sherbet tower was obtained, sampling for microscopic observation was done after mixing the tower for 15 minutes at 150 rpm agitation.

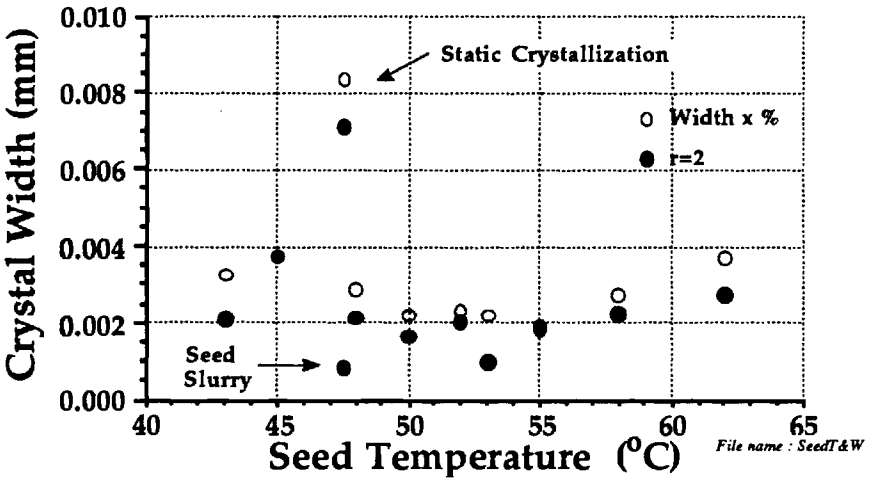

Figure 32: Effect of Seeding on APM Crystal Width at a Cooling Rate of 60°C/h

Results

Table 4 gives the data from the experiments, and Figure 32 shows the effect of seed temperature on the resulting APM crystal width. Also shown in the figure are results from static crystallization which produced APM crystals of about 0.008 mm width whereas all seeded experiments produed crystals having an average width of about 0.002 mm, a factor of 4 smaller. The initial APM concentration of 42 g/L H_2O corresponds to a saturation temperature of 62.0°C. Spontaneous nucleation in the unseeded static crystallization of such systems is expected to occur at 45.6±1.75°C. The APM crystals obtained were also about twice as large as the seed crystals added to the crystallizer.

Crystals in the seed slurry were scattered throughout the APM solution, but within about 1 minute every seed crystal stopped its movement and remained the same size. Although from the point of view of mixing, the procedure coresonded to static crystallization, the resulting crystals had a much different appearance. Instead of hedgehog-like crystal growth, which typically produces the bundle crystals in static crystallization, huge numbers of tiny crystals appeared with the addition of the seed crystal slurry. Although the conditions does not correspond to those usually expected with initial breeding, it is apparent that some form of secondary nucleation is leading to the production of larger numbers of crystals.

These results indicate that crystals obtained from agitated crystallization cannot be used to seed a static process to obtain large bundle crystals.

File name	Seed Added Temp.(C)	Solv.at Seed Addition	Sigma at Seed Addition	Width Ratio x Width	Gamma Dist. r=1	m1	m2	r=2	m1	m2	r=3	m1	m2	r=4	m1	m2
921201V4	43	20.851	1.014	3.2417E-03				2.0995E-03	9.5262E+02	2.9309E+03	2.1016E-03	1.4275E+03	3.4395E+03			
								0.88742			0.86714					
				100				*64.77*			*64.83*					
921117V1	45	22.448	0.871	3.7340E-03				3.7287E-03	5.3638E+02	2.6706E+03	3.5449E-03	8.4629E+02	3.0720E+03			
								0.76931			0.77085					
				100				*99.86*			*94.94*					
921117V2	48	25.076	0.675	2.8380E-03				2.1558E-03	9.2772E+02	2.3030E+03	2.2425E-03	1.3378E+03	2.7235E+03			
								0.85988			0.85632					
				100				*75.96*			*79.02*					
921113V2	50	26.997	0.556	2.1743E-03	1.3486E-03	7.4166E+02	1.1281E+03	1.6522E-03	1.2105E+03	1.6609E+03	1.7769E-03	1.6884E+03	2.0062E+03			
					0.74282			0.76962			0.79309					
				100	*62.02*			*75.99*			*81.72*					
921201V2	52	29.065	0.445	2.3100E-03				2.0218E-03	9.8922E+02	2.3523E+03	2.0506E-03	1.4630E+03	2.6577E+03			
								0.77658			0.81751					
				100				*87.52*			*88.77*					
921201V3	53	30.158	0.393	2.1852E-03	6.6970E-04	1.4932E+03	5.6204E+02	9.6340E-04	2.0759E+03	1.0120E+03						
					0.96025			0.95345								
				100	*30.65*			*44.09*								
921113V1	55	32.468	0.294	1.7667E-03				1.9077E-03	1.0484E+03	4.2967E+03	1.7797E-03	1.6857E+03	5.0281E+03			
								0.633385			0.6838					
				100				*107.98*			*100.74*					
921116V2	58	36.269	0.158	2.7474E-03				2.2219E-03	9.0013E+02	2.2537E+03	2.2817E-03	1.3148E+03	2.6617E+03			
								0.806831			0.803663					
				100				*80.87*			*83.05*					
921116V1	60	39.047	0.076	3.5488E-03				2.8648E-03	6.3814E+02	2.6138E+03	2.9892E-03	1.0036E+03	2.9913E+03	2.8907E-03	1.3837E+03	3.2628E+03
								0.6622195			0.6959			0.7189		
				100				*80.73*			*84.23*					
921201V1	62	42.038	-0.001	3.6773E-03				2.7216E-03	7.3487E+02	2.7905E+03	2.7280E-03	1.0997E+03	3.2668E+03			
								0.88646			0.86621					
				100				*74.01*			*74.18*					
921012 (Agit.Slurry)	48.5	25.543	0.644	9.0252E-04				8.3034E-04	2.4086E+03	3.7705E+03	8.6015E-04	3.4878E+03	4.4116E+03			
								0.68234			0.71408					
				100				*92.00*			*95.31*					
920918V2 (Blank)	47.5	24.618	0.706	8.4506E-03				7.0647E-03								
930128V3 (Blank)	45.1	22.531	0.864	5.7998E-03				5.1089E-03								
930309V1 (Blank)	42.5	20.470	1.052	5.4591E-03				3.0926E-03								
930310V2 (Blank)	44.3	21.876	0.920	7.3979E-03				6.3308E-03								

Table 4. Seeded Static Crystallization with a Cooling Rate of 60oC/h and an Initial Concentration of 42.0 g/L

12 Literature Cited

European Patent Application Number 0091787, 1985.

S. Kishimoto and M. Naruse, "The 'bundling' phenomenon in aspartame crystallization," *Chemistry and Industry*, 127–128, February 16, 1987.

S. Kishimoto, N. Nagashima, M. Naruse and K. Toyokura, "The 'Bundle-Like' Crystals in Aspartame Crystallization," *Industrial Crystallization 87*, J. Nyvlt and S. Zcek, eds., Elsevier, Amsterdam, 511–514, 1989a.

S. Kishimoto, H. Ohura, M. Naruse and K. Toyokura, "Crystallizer Development for the Bundle Aspartame Crystals," *Industrial Crystallization 87*, J. Nyvlt and S. Zcek, eds., Elsevier, Amsterdam, 515–518, 1989b.

R. C. Zumstein and R. W. Rousseau, "Agglomeration of Copper Sulfate Pentahydrate Crystals within Well-Mixed Crystallizers," *Chemical Engineering Science*, **44**, 2149–2155(1989a).

R. C. Zumstein and R. W. Rousseau, "The Influence of Surfactants on the Crystallization of L-Isoleucine," *Industrial & Engineering Chemistry Research*, **28**, 334–340(1989b).